School of Chemical and Petroleum Engineering

Department of Chemical Engineering

Magnetic nanocatalysts for oxidative decomposition of persistent organic pollutants (POPs) in contaminated water

Yilin Liu

This thesis is presented for Degree of

Master of Philosophy (Chemical Engineering)

Of

Curtin University

August 2015

Declaration

To the best of my knowledge and belief this thesis contains no material previously published by any other person except where due acknowledgment has been made. This thesis contains no material which has been accepted for the award of any other degree or diploma in any university.

Signature: Yilin Liu Date: 6 Aug 2015

Acknowledgement

I would like to express my sincere gratitude to my supervisor, Professor Shaobin Wang, for his selfless and continuous supports of my master study and research. I had no chance to complete this thesis without his intelligence and warm encouragement.

I am also grateful to my co-supervisor, Dr. Hongqi Sun whose knowledge always gives me inspiration and helps me to make everything possible during my postgraduate years.

My sincere gratitude must go to Mr. Yuxian Wang and Xiaoguang Duan who are always ready to help me at various occasions.

I am also thankful to all laboratory technical staff, Karen Haynes, Jason Wright, Ann Carrol and Roshanak Doroushi for their kindly technical support.

And last, but not the least, I would like to thank my parents for everything they give me. They support everything I want and I must say that I have the best parents in the world.

Abstract

In the past decades, applications of advanced oxidation processes (AOPs) for persistent organic pollutants (POPs) treatment in wastewater have been thoroughly investigated. The AOPs can improve biodegradability of pollutants and they are useful for cleaning biologically toxic and non-degradable materials in waste water. Among these processes, the sulfate radical-based reaction has been employed as a low-cost, environmentally-friendly and sustainable technique to purify wastewater.

The aim of this work is to synthesize different magnetic nanocatalysts by a hydrothermal method which can present high activity and good magnetic performance in the oxidation of phenol solutions. Three types of catalysts were synthesized with either one-pot or two-step hydrothermal method. All of these synthesized catalysts were examined for peroxymonosulfate (PMS, Oxone) activation for the decomposition of phenol.

In all the catalysts, the magnetic carbon nanospheres supported Mn nanoparticles which were synthesized by a one-pot hydrothermal method and self-reduction in N_2 atmosphere with the carbon from hexamethylenetetramine (HMTA) showed the best oxidizing ability which could give effectively phenol decomposition in about 42 minutes.

Contents

1. Introduction and Overview

1.1 Motivation

During the last several years, how to reduce environmental pollutants has been a serious issue[1]. To deal with this problem, a lot of researchers have shown interest in the production of environmentally-friendly materials and treatment techniques[2]. Normally, the pollutants include two kinds of contaminations: water and solid pollution[3], which can not only reduce the availability of fertile land for agricultural use but also pose a risk to public health[4], food system[5] and groundwater[6]. As one kind of most serious pollutant, persistent organic pollutants (POPs) have attracted particular concern for their long life-time, toxicity and resistance against nature attenuation[7].

To provide satisfied POPs degradation, advanced oxidation processes (AOPs) have been considered to be one of the most effective treatments due to their ability of fully degradation of POPs[8]. They also support a new path for novel technology. Numerous studies have been reported to use magnetic catalysts to activate OXONE (potassium monopersuphate) for oxidation of POPs in soil and water[9]. The magnetic catalysts have attracted great attention due to their high specific surface area[10], unique size[11] and morphology-dependent physical and chemical properties[12].

1.2 Objectives of thesis

The main objective of this research is to synthesize a new kind of magnetic nanocatalyst by a novel hydrothermal method which can appear high activity and good magnetic performance in the reaction of oxidizing phenol solutions.

1.3 Thesis organization

Chapter one briefly introduced the major technique for removal of persistent organic pollutants. Chapter two presented a comprehensive literature review on pollutant removal techniques in four aspects: the methods of water pollution control, the classification of AOPs, the classification of catalysts and the introduction of magnetic nanocatalysts. Chapter three described a one-pot hydrothermal method to synthesize the carbon nanospheres supported by Mn catalysts with glucose to supply the carbon elementary substances. Chapter four showed a two-step hydrothermal method to synthesize the carbon nanospheres supported by Mn catalysts with glucose to supply the carbon elementary substances. Chapter five showed a one-pot hydrothermal method to synthesize the carbon nanospheres supported by Mn catalysts with hexamethylenetetramine to supply the carbon elementary substances. Chapter six summarized the overall thesis and discussed the performance of all the materials which were synthesized during the research work for organic degradation. The final part of this chapter was devoted to the possible suggestions and future work.

1.4 References

1. Arslan, I.; Balcioglu, I. A.; Tuhkanen, T.; Bahnemann, D., H2O2/UV-C and Fe2+/H2O2/UV-C versus TiO2/UV-A treatment for reactive dye wastewater. Journal of Environmental Engineering-Asce 2000, 126 (10), 903-911.

2. (a) Chen, J.; Wang, X.; Liu, X.; Huang, J.; Xie, Z., Removal of Dye Wastewater COD by Sludge Based Activated Carbon. Journal of Coastal Research 2015, 1-3; (b) Chen, Z.; Zayed, T.; Qasem, A., An Efficiency-Centred Hierarchical Method to Assess Performance of Wastewater Treatment Plants. International Journal of Environmental Research 2015, 9 (1), 1-8; (c) Guo, J.; Peng, Y.; Ni, B.-J.; Han, X.; Fan, L.; Yuan, Z., Dissecting microbial community structure and methane-producing pathways of a full-scale anaerobic reactor digesting activated sludge from wastewater treatment by metagenomic sequencing. Microbial cell factories 2015, 14 (1), 218-218; (d) Lee, O. M.; Kim, H. Y.; Park, W.; Kim, T.-H.; Yu, S., A comparative study of disinfection efficiency and regrowth control of microorganism in secondary wastewater effluent using UV, ozone, and ionizing irradiation process. Journal of hazardous materials 2015, 295, 201-8.

3. Nasrabadi, T., An Index Approach to Metallic Pollution in River Waters. International Journal of Environmental Research 2015, 9 (1), 385-394.

4. Ahmad, K.; Khan, Z. I.; Ashfaq, A.; Ashraf, M.; Akram, N. A.; Yasmin, S.; Sher, M., Assessment of Heavy Metals and Metalloids in Solanum tuberosum and Pisum sativum Irrigated with Urban Wastewater in the Suburbs of Sargodha City, Pakistan. Human and Ecological Risk Assessment 2015, 21 (4), 1109-1122.

5. Asgari, K.; Cornelis, W. M., Heavy metal accumulation in soils and grains, and health risks associated with use of treated municipal wastewater in subsurface drip irrigation. Environmental monitoring and assessment 2015, 187 (7), 4565-4565.

6. Matamoros, V.; Gutierrez, R.; Ferrer, I.; Garcia, J.; Bayona, J. M., Capability of microalgae-based wastewater treatment systems to remove emerging organic contaminants: A pilot-scale study. Journal of Hazardous Materials 2015, 288, 34-42.

7. Thangavadivel, K.; Megharaj, M.; Smart, R. S. C.; Lesniewski, P. J.; Naidu, R., Application of high frequency ultrasound in the destruction of DDT in contaminated sand and water. Journal of Hazardous Materials 2009, 168 (2-3), 1380-1386.

8. Sable, S. S.; Ghute, P. P.; Alvarez, P.; Beltran, F. J.; Medina, F.; Contreras, S., FeOOH and derived phases: Efficient heterogeneous catalysts for clofibric acid degradation by advanced oxidation processes (AOPs). Catalysis Today 2015, 240, 46-54.

9. Wang, Y.; Sun, H.; Ang, H. M.; Tade, M. O.; Wang, S., Magnetic Fe3O4/carbon sphere/cobalt composites for catalytic oxidation of phenol solutions with sulfate radicals. Chemical Engineering Journal 2014, 245, 1-9.

10. Fang, Q.; Cheng, Q.; Xu, H.; Xuan, S., Monodisperse magnetic core/shell microspheres with Pd nanoparticles-incorporated-carbon shells. Dalton Transactions 2014, 43 (6), 2588-2595.

11. Park, H. H.; Woo, K.; Ahn, J.-P., Core-Shell Bimetallic Nanoparticles Robustly Fixed on the Outermost Surface of Magnetic Silica Microspheres. Scientific Reports 2013, 3.

12. Guo, H.; Liu, X.; Hou, Y.; Xie, Q.; Wang, L.; Geng, H.; Peng, D.-L., Magnetically separable and recyclable urchin-like Co-P hollow nanocomposites for catalytic hydrogen generation. Journal of Power Sources 2014, 260, 100-108.

2. Literature Review

2.1 Introduction

Due to increasingly fast pace of global industrialization and lacking in the awareness of environmental protection, water and soil contamination has become a critical issue worldwide. The contaminated sites not only reduce the availability of fertile land for agricultural use but also pose a risk to public health, food system and groundwater. Among the pollutants discharged from industrial sites, contaminants in terms of persistent organic pollutants (POPs) have attracted particular concern owing to their long life-time, toxicity, and resistance against nature attenuation[1] . The chemical characteristics of POPs are generally recognised as carcinogenic polycyclic aromatic hydrocarbons (PAHs) and certain brominated flame-retardants, as well as some organo-metallic compounds such as tributyltin (TBT). Therefore, in order to protect the safety of both animals and human beings' as well as to prevent deterioration of water quality, it is crucial and imperative to treat wastewater and eliminate these organic contaminates before its discharging to the environment. Being hydrophobic, these POPs adsorb strongly on soil texture, making them very difficult to treat, especially in low permeable clayey soil[2]. As a result, conventional wastewater treatment techniques based on the primary and secondary treating such as activating sludge treatment fail to achieve a satisfied POPs degradation rate. In addition, conventional mechanical-biological purification no longer suffices and must be supplemented by additional stages of processing.

To provide satisfied POPs degradation, advanced treatment processes have been developed, including advanced oxidation processes (AOPs), wet air oxidation (WAO) and membrane processes, such as ultra-filtration, nano-filtration, and hyper-filtration, in which physical processes can only transfer the pollutants from one phase to another. However, these methods significantly depend on pH (Fenton reaction), energy input (Ozone-UV, ultrasound, electrokinetic, supercritical oxidation process (SCWO), and thermal treatment), and operating

period (bioremediation and photo-remediation).[3] There is an urgent need to develop novel technologies to treat water and soil contaminated by POPs.

Recently, nanotechnologies have shown their great potential for treatment of waste water, contaminated soil, and air pollution. The available nanomaterials that have been applied in the treatment of POPs include nano zero-valent iron (ZVI) as permeable soil barriers (PRBs)[4], mesoporous nanomaterials as adsorbents[5], and nanosized photocatalysts for AOPs[6]. Nevertheless, the main barrier of nanotechnologies hindering their large-scale application is the recovery approach of used nanomaterials[7], especially in soil remediation cases in which the only choice of centrifugation is no longer practical due to the co-sedimentation nature of soil. Moreover, if not well recovered, the catalysts would bring secondary contamination to water or soil which could be more serious than the primary one.

A promising strategy for resolving the problem is recovery by magnetic separation. Nanoparticles (or quantum dots) can be fabricated on a magnetically separable support to make the nanocatalysts separable by a magnetic field[8]. γ-Fe_2O_3 or magnetite Fe_3O_4 in 10 – 20 nm exhibits a special form of magnetism called superparamagnetism. Inert barrier materials (< 100 nm) can be fabricated to encapsulate the γ-Fe_2O_3 or magnetite Fe_3O_4 for protecting the ferromagnetic nanoparticles, and then loaded with catalysts for applying reaction and the magnetic platform.

The application of Fenton reaction requires a low pH (~3), which in turn creates other issues to deal with the acid solution. Sulfate radicals which could be produced by sulfate based oxidants have been suggested as an alternative due to their higher oxidation potential[9]. More importantly, the generation of sulfate radical will also be superior to Fenton reaction by the potentials applied in a wide range of pHs for the generation of sulfate radical[10]. The prepared

magnetically separable catalysts will be used to activate OXONE (potassium monopersuphate) for oxidation of POPs in soil and water.

It has been found that cobalt ions are effective for oxone activation to provide sulfate radicals. The radical generation and organic degradation processes can be described as below.

$$Co^{2+} + HSO_5^- \rightarrow Co^{3+} + SO_4^{\bullet -} + OH^- \quad (1)$$

$$SO_4^{\bullet -} + H_2O \rightarrow SO_4^{2-} + OH^{\bullet} + H^+ \quad (2)$$

$$SO_4^{\bullet -} + \text{organics} \rightarrow \xrightarrow{\text{several steps}} CO_2 + H_2O \quad (3)$$

However, the major issue confronting cobalt based oxidation technique is the toxicity of cobalt ion. Cobalt is recognized as a priority pollutant in water, which leads to several health problems such as asthma, pneumonia and other lung problems. In order to restrict the discharge of cobalt ions, it has been proposed to employ a heterogeneous cobalt catalyst by supporting the cobalt ions on a solid surface for oxidation. Previously, several types of heterogeneous Co catalyst including Co oxides[11], Co composites[12] and supported Co catalysts have been investigated[13].

In addition to cobalt-based catalysts, recent studies also reveal that graphene which is a form of nanocarbons, can effectively activate PMS for producing sulphate radicals. The activity of graphene is higher than graphite powder (GP), activated carbon (AC), carbon nanotube (CNT), and graphene oxide (GO). Moreover, graphene is able to degrade phenol, dichlorophenol (DCP) and methylene blue (MB) more efficiency than a typical cobalt catalyst, Co_3O_4 nanoparticles[14]. It is suggested that the chemical properties of graphene is exceptionally sensitive to the lattice imperfections[15,16]. And numerous simulations indicate that hydroxyl, carboxyl, or other groups can easily be attached to vacancy-type defects. Simulations also show that reconstructed defects without dangling bonds such as SW defects or reconstructed vacancies locally change the density of electrons and may also increase the

local reactivity. And it can be inferred that these defects can act as catalytic centres for PMS activation reaction.

Recently, it has been found that nanoscale ZVI could show a higher activity in reduction reactions, when compared to conventional microscale ZVI particles[17, 18 and 19]. Nano scaled Fe^0 generally offers high surface-area-to-volume ratios, high specific surface area, and high surface reactivity. Instead of using the expensive borohydride salt as the reducing agent, Hoch et al.[20]reported that ZVI nanoparticles could be prepared by the reduction of carbon black, which was also used as a support material, under Ar flow at a calcination of above 600 °C. Since ZVI nanoparticles favour strong aggregation into microscale particles due to the high surface energy and intrinsic magnetic interaction, support such as polystyrene resin[21], alumina[22], bentonite[23], kaolinite[24], zeolite[25], carbon black[20], activated carbon[26], carbon nanotubes[27], and carbon spheres is required for better Fe^0 distribution. Another concern of nano-Fe^0 is its instability in air. Due to high surface energy, ZVI nanoparticles can easily react with the oxygen within the air and form more stable iron oxide. Encapsulation of nano-Fe^0 into porous carbon spheres is suggested to be a promising way for enhancement of transportation, suspension, and stability of nanoscaled ZVI without significantly sacrificing activity.

Hausmannite (Mn_3O_4) has drawn particular research attention because of its distinctive structure and physicochemical properties, which are of great interest in energy conversion, magnetics, and catalysis, etc.[28,29]. Despite the high catalytic performance of Mn_3O_4 nanoparticles (NPs), its poor chemical and thermal stabilities, which could lead to aggregation of NPs, not only decreases the catalytic efficiency but limits its wider application. To solve this, carbonaceous materials with high electrical conductivity and buffer matrix have been widely employed as supports for Mn_3O_4-based catalysts to improve their conductivity and stability[30].

Besides hausmannite, other form of manganese oxide-MnO_2 also shows its potential as a catalyst in wastewater treatment. Previously, MnO_2 was usually used for the Fenton-like reaction for production of hydroxyl radicals from H_2O_2 and oxidation of organic compounds. Anipsitakis and Dionysiou[31] studied nine transition metal ions for the activation of three oxidants and the generation of sulfate, peroxymonosulfate, and hydroxyl radicals. They suggested that the conjunction of Mn^{2+} ions were capable of generation of sulfate radicals by activation of peroxymonosulfate.

2.2 The overview of water pollutions

During the last decades, water environment has suffered from the increasingly heavy pollution burden caused by population increase and economic development. After the water has been polluted, it affects people's life. According to the World Health Organization (WHO), 1.8 million people died by drinking the polluted water. To be exact, probably 1/6 of the world's population is suffering from unsafe water, especially in the developing countries[28].

Chemical products are one of the most dangerous pollutants which have caused a large number of water-pollution accidents[32]. For example, as one of the most famous river, Songhua River experienced a serious accident caused by benzene and nitrobenzene products[31]. Among the pollutants discharged from industrial sites, contaminants in terms of persistent organic pollutants (POPs) have attracted particular concern owing to their long life-time, toxicity, and resistance against nature attenuation[1]. The chemical characteristics of POPs are generally recognised as carcinogenic polycyclic aromatic hydrocarbons (PAHs) and certain brominated flame-retardants, as well as some organo-metallic compounds such as tributyltin (TBT)[33].

2.3 The methods of water pollution control

In order to protect the human being's safety, a huge number of researches have been devoted to achieving a reasonable solution to protect the water environment. As a viable method, influence factors and economy should be two important points which can value the benefits of the projects[34], such as the agricultural water pollution control's applications[35], water supply system's technology innovation[36], and comprehensive economic assessment's water environmental model[37].

Besides the previous approaches, the advanced oxidation processes (AOPs) have been considered to be one of the most effective treatments because of the ability of fully degradation of the POPs[38]. The AOPs can improve the pollutants' biodegradability and they are useful for cleaning biologically toxic and non-degradable materials such as aromatics, petroleum constituents and volatile organic compounds in waste water[39].

2.4 The classification of AOPs

Advanced oxidation processes, to put it simple, refer to a series of chemical treatment procedures which are designed to remove organic or inorganic materials in waste water by supplying hydroxyl radicals with high oxidizability[40]. According to the methods of producing free radicals and difference of reaction conditions, the AOPs can be classified as six aspects: photochemical oxidation, catalytic wet-air oxidation, acoustic chemical oxidation, ozone oxidation, electrochemical oxidation and Fenton oxidation.

Photochemical oxidation is the reaction of a chemical change in a substance which caused it to lose electrons initiated by light[41]. A common example is photochemical smog which is caused by hydrocarbons and NO_x reacting under the influence of UV light[42]. It can be used in contaminated water, air and solids treatments for its high oxidizing ability and gentle reaction

conditions[43]. However, photochemical oxidation is easy to produce aromatic compounds which can lead to organics' halfway degradation for its limitation of reaction conditions, this problem is the one which should overcome first[44].

The method of catalytic wet-air oxidation is a process which can decompose the organic pollutants to carbon dioxide and nitrogen by activating oxygen species which can take place of high temperatures and pressures[45]. It is known for its capacities which can break biologically refractory compounds to simpler treated materials before they are being released[46]. However, drawbacks do exist for its inability to get deeply mineralization of organics pollutants because of certain low molecular weight oxygenated compounds, such as acetic, propionic and acetaldehyde can present in waste water during the process of oxidation, which are hard to further transform to carbon dioxide[46]. For example, when the temperature is lower than 573K, it is hard to remove acetic acid from waste water[47].

The method of acoustic chemical oxidation is a process of using ultrasonic wave to speed up the reaction or activate new reaction in order to increase chemical efficiency[48]. It is well known for good applicability[49] and development in combining with other technologies[50]. The disadvantages of this method are high cost[51] and low energy efficiency[52].

The method of ozone oxidation is an oxidation process which is achieved by two approaches: direct reaction[53] and indirect reaction[54]. Direct reaction is efficiency for unsaturated aliphatic hydrocarbons and aromatic hydrocarbons by the reaction of ozone and organics[55]. Indirect reaction is a process which ozone can decompose –OH to react with organics[56]. Ozone oxidation is well known for its high ability of decolourization[57] and organic pollutions removal[58]. However, drawbacks do exist. The high cost[59] and easily to decompose intermediate products[60] which can stop the oxidating process of ozone are two main disadvantages. Therefore, there is big boundedness for this method to treat in organic pollutions degradation.

The method of electrochemical oxidation is an oxidation process which is achieved by oxidating electrode reaction to the purification of waste water[61]. It can divide into two sections as well: direct reaction[62] and indirect reaction[63]. Direct action can purify the waste water by releasing –OH to adsorb the organics[64]. Indirect reaction can purify the waste water by the oxidation of C_{12} and C_{10} in the solution[65]. This method is well known for its good efficiency of removal of COD and NH_3-N from the waste water[66]. The main disadvantage is that there will be large energy consumption for this method operating[67].

The method of Fenton oxidation is an advanced oxidation technology, this method can oxidate a huge number of toxic and refractory organics by using the strong oxidizing –OH which formed by the reaction of Fe and H_2O_2[68]. The influence factors are pH[68], the input of H_2O_2 and ferric chloride[69]. It is efficient for the oxidation of refractory organics[70]. However, drawbacks do exist. The main disadvantages are high cost[71] and difficulty of catalyst reactivation[72].

2.5 The classification of catalysts

A catalyst is a material which can speed up a reaction's rate[73]. With a catalyst, reactions can be faster with less energy[74]. Catalysts are one of the most important chemicals as it only requires less energy to reach the transition rate[75]. A catalyst works by supporting an alternative reaction pathway to the reaction product. The catalysts can be classified in three aspects: heterogeneous catalysts, homogeneous catalysts and biocatalysts[76].

Heterogeneous catalysts can be used in different phase than the reactants which means the reactants under catalysis are in different states[77]. For example, when producing the butter, unsaturated vegetable oil and nitrogen can be transformed to saturated fat by using the catalyst of solid nickel[78]. Solid nickel is one kind of heterogeneous catalysts, and the reactants which are catalysed are vegetable oil and nitrogen[79].

Heterogeneous catalysts are typically "supported," which means that the catalyst is dispersed on a second material that enhances the effectiveness or minimizes their cost. Supports prevent or reduce agglomeration and sintering of the small catalyst particles, exposing more surface area, thus catalysts have a higher specific activity (per gram) on a support[80]. Sometimes the support is merely a surface on which the catalyst spread to increase the surface area. More often, the support and the catalyst interact, affecting the catalytic reaction. Supports are porous materials with a high surface area, most commonly alumina, zeolites or various kinds of activated carbon[81]. Specialized supports include silicon dioxide, titanium dioxide, calcium carbonate, and barium sulfate[82].

When the catalysts and reactants are in the same phase, and there is no reaction on the phase boundary, we call it homogeneous reaction, and the catalysts are homogeneous catalysts[83]. It includes liquid acid and alkali, ksetra-ksetrajna solid acid and alkali and soluble transition metal compounds[84]. Homogeneous catalysts are reacted independently by molecules or ions, their advantages are flat active centre, high activity and high selectivity[85].

The biocatalysts are catalytic organics which are produced by plants, animals and microbial[86]. Biocatalysts can be thought of as intermediate between homogeneous and heterogeneous catalysts[87]. The activities of biocatalysts can be affected by a lot of factors which include temperature[88], pH[89], substrate[90] and concentration of enzyme[91]. Water is one of the most important reagents in biocatalysts reactions, because water is the product of many bond-forming reactions and many bond-breaking processes' reactant[92].

Catalysts play important roles in producing chemical products, such as chemical fertilizer, pesticide and chemical raw materials[93]. From the Boltzmann distribution and energy profile diagram, we can find that, catalysts can activate reactions with less activation energy in the situation that reactants are unchangeable[94].

Catalysts can be useful with little amount, it is better to use mixed catalysts[95]. Because most

of inorganic acid and alkali catalysts are corrosion and poisonous[96], for the organic catalysts, most of them are inflammable, flammable and poisonous[97]. For example, boron trifluoride-ethylether complex is highly toxic organic catalyst, it is important to store and use it safely[98]. Among the various of catalysts, magnetic nanocatalysts attract much more focus[99]. The magnetic nanocatalyst is one kind of catalyst which is loaded to magnetic media, it is easy to recycle and reuse[100]. In the following chapter, I will show you more details of magnetic nanocatalysts.

2.6 The literature review of magnetic nanocatalysts

In this chapter, I will show you an overview of the development of magnetic nanocatalysts in several areas, such as oxidation catalysis, esterification reaction catalysis, photocatalysis and so on. The purpose is discussing the preparation methods of magnetic nanocatalysts and presenting the problems during the practical application.

2.6.1 The features of magnetic nanocatalysts

The main features of magnetic nanocatalysts are as follows:

1) The specific surface area of magnetic nanocatalyst is high. With the increase of specific surface area, the particle surface function group, density of active sites and the ability of preferential adsorption are increase as well, which will give rise to higher loading capacity on catalytic activity groups[101].
2) The magnetic nanocatalysts' catalytic active sites can be uniform distributed on the surface of the nanoparticles, which can avoid the diffused the carrier pores of the general catalysts[102].
3) The magnetic nanocatalysts can disperse uniformly in the liquid phase because their tiny sizes. Therefore, the catalytic activity groups on the surface of the particles can react with the reactants easier[103].

4) The magnetic nanocatalysts have the feature of magnetic responsiveness, with the external magnetic field, they can be easily separate and recycle[104].
5) The magnetic nanocatalysts have higher stability in most reaction systems[105].

2.6.2 The application of magnetic nanocatalysts in oxidizing reactions

Alcohols and olefins' oxidizing reaction is one of the most important reactions, the reaction products are important raw materials of fine chemicals[106]. As a perfect catalyst in oxidizing reaction, magnetic nanocatalyst is good for its small particle size[107], big specific surface area[108], good dispersivity[109] and good contact with reactants. Mohsen et.al used urea-hydrogen peroxide as the oxidizing agent and Ni on MCM-41 as catalyst to oxidize sulphides to sulfoxides; this method could successfully oxidize a variety of aromatic and aliphatic sulphides and thiols with short reaction time at room temperature[105].

2.6.3 The application of magnetic catalysts in esterification reactions

In the last several years, with the development of the research of solid acid catalysis, magnetic solid acid catalysts have the features of easily recycle and separate[110]. Jing et.al synthesized three component magnetic solid nanocatalysts TiO_2-Al_2O_3-Fe_3O_4, CeO_2-Al_2O_3-Fe_3O_4 and ZrO_2-Al_2O_3-CeO_2-Fe_3O_4 with a method of co-precipitation, these three catalysts demonstrated good catalytic activity[111].

2.6.4 The application of magnetic catalysts in photocatalysis

As a technology to treat the pollution, heterogeneous photocatalytic semiconductor attract more and more attention[112]. Yu et.al used a solvent evaporation combined with a facile inner-pore hydrolysis to decorate mesoporous silica, and then preloaded the gamma-Fe_2O_3

nanoparticles to SBA-15[113]. The composites remain comparable and adsorption in the second use, demonstrating the perfect stability of the composites[113].

2.6.5 The significance and development of magnetic nanocatalysts

From the previous chapters, we can find magnetic nanocatalysts are better than traditional catalysts in several aspects, such as activity[114], conversion ratio[115] and selectivity[116]. Nowadays, the research of magnetic nanocatalysts is still in the early days. For example, the effects of preparation conditions on surface properties of the carrier[117], saturated magnetization and the stability of catalytic activity groups still need further study[80]. For this thesis, it will present a new method to synthesize different magnetic nanocatalysts by a hydrothermal method that can present high activity and good magnetic performance in the oxidation of phenol solutions.

2.7 References

1. Thangavadivel, K.; Megharaj, M.; Smart, R. S. C.; Lesniewski, P. J.; Naidu, R., Application of high frequency ultrasound in the destruction of DDT in contaminated sand and water. *Journal of Hazardous Materials* **2009,** *168* (2-3), 1380-1386.

2. Pham, T. D.; Shrestha, R. A.; Virkutyte, J.; Sillanpaa, M., Combined ultrasonication and electrokinetic remediation for persistent organic removal from contaminated kaolin. *Electrochimica Acta* **2009,** *54* (5), 1403-1407.

3. Fertu, D. I. T.; Gavrilescu, M., APPLICATION OF NATURAL ZEOLITES AS SORBENTS IN THE CLEAN-UP OF AQUEOUS STREAMS. *Environmental Engineering and Management Journal* **2012,** *11* (4), 867-878.

4. Zhang, L. D.; Fang, M., Nanomaterials in pollution trace detection and environmental improvement. *Nano Today* **2010,** *5* (2), 128-142.

5. Liu, G. H.; Wang, J. L.; Zhu, Y. F.; Zhang, X. R., Application of multiwalled carbon nanotubes as a solid-phase extraction sorbent for chlorobenzenes. *Analytical Letters* **2004,** *37* (14), 3085-3104.

6. Yang, L. X.; Luo, S. L.; Liu, R. H.; Cai, Q. Y.; Xiao, Y.; Liu, S. H.; Su, F.; Wen, L. F., Fabrication of CdSe Nanoparticles Sensitized Long TiO(2) Nanotube Arrays for Photocatalytic Degradation of Anthracene-9-carbonxylic Acid under Green Monochromatic Light. *Journal of Physical Chemistry C* **2010,** *114* (11), 4783-4789.

7. Xuan, S. H.; Jiang, W. Q.; Gong, X. L.; Hu, Y.; Chen, Z. Y., Magnetically Separable Fe(3)O(4)/TiO(2) Hollow Spheres: Fabrication and Photocatalytic Activity. *Journal of Physical Chemistry C* **2009,** *113* (2), 553-558.

8. Shylesh, S.; Schunemann, V.; Thiel, W. R., Magnetically Separable Nanocatalysts: Bridges between Homogeneous and Heterogeneous Catalysis. *Angewandte Chemie-International Edition* **2010,** *49* (20), 3428-3459.

9. Anipsitakis, G. P.; Dionysiou, D. D., Radical generation by the interaction of transition metals with common oxidants. *Environmental Science & Technology* **2004,** *38* (13), 3705-3712.

10. Anipsitakis, G. P.; Dionysiou, D. D.; Gonzalez, M. A., Cobalt-mediated activation of peroxymonosulfate and sulfate radical attack on phenolic compounds. Implications of chloride ions. *Environmental Science & Technology* **2006,** *40* (3), 1000-1007.

11. Anipsitakis, G. P.; Stathatos, E.; Dionysiou, D. D., Heterogeneous activation of oxone using Co3O4. *Journal of Physical Chemistry B* **2005,** *109* (27), 13052-13055.

12. Do, S. H.; Jo, J. H.; Jo, Y. H.; Lee, H. K.; Kong, S. H., Application of a peroxymonosulfate/cobalt (PMS/Co(II)) system to treat diesel-contaminated soil. *Chemosphere* **2009,** *77* (8), 1127-1131.

13. Saputra, E.; Muhammad, S.; Sun, H. Q.; Ang, H. M.; Tade, M. O.; Wang, S. B., Red mud and fly ash supported Co catalysts for phenol oxidation. *Catalysis Today* **2012,** *190* (1), 68-72.

14. Wang, S. B.; Sun, H. Q.; Ang, H. M.; Tade, M. O., Adsorptive remediation of environmental pollutants using novel graphene-based nanomaterials. *Chemical Engineering Journal* **2013,** *226*, 336-347.

15. Britnell, L.; Gorbachev, R. V.; Jalil, R.; Belle, B. D.; Schedin, F.; Katsnelson, M. I.; Eaves, L.; Morozov, S. V.; Mayorov, A. S.; Peres, N. M. R.; Neto, A. H. C.; Leist, J.; Geim, A. K.; Ponomarenko, L. A.; Novoselov, K. S., Electron Tunneling through Ultrathin Boron Nitride Crystalline Barriers. *Nano Letters* **2012,** *12* (3), 1707-1710.

16. Geim, A. K.; Novoselov, K. S., The rise of graphene. *Nature Materials* **2007,** *6* (3), 183-191.

17. Ryu, A.; Jeong, S. W.; Jang, A.; Choi, H., Reduction of highly concentrated nitrate using nanoscale zero-valent iron: Effects of aggregation and catalyst on reactivity. *Applied Catalysis B-Environmental* **2011,** *105* (1-2), 128-135.

18. Song, H.; Carraway, E. R., Reduction of chlorinated ethanes by nanosized zero-valent iron: Kinetics, pathways, and effects of reaction conditions. *Environmental Science & Technology* **2005,** *39* (16), 6237-6245.

19. Joo, S. H.; Feitz, A. J.; Waite, T. D., Oxidative degradation of the carbothioate herbicide, molinate, using nanoscale zero-valent iron. *Environmental Science & Technology* **2004,** *38* (7), 2242-2247.

20. Zhan, J. J.; Zheng, T. H.; Piringer, G.; Day, C.; McPherson, G. L.; Lu, Y. F.; Papadopoulos, K.; John, V. T., Transport Characteristics of Nanoscale Functional Zerovalent Iron/Silica Composites for in Situ Remediation of Trichloroethylene. *Environmental Science & Technology* **2008,** *42* (23), 8871-8876.

21. Du, Q.; Zhang, S. J.; Pan, B. C.; Lv, L.; Zhang, W. M.; Zhang, Q. X., Bifunctional resin-ZVI composites for effective removal of arsenite through simultaneous adsorption and oxidation. *Water Research* **2013,** *47* (16), 6064-6074.

22. Karabelli, D.; Unal, S.; Shahwan, T.; Eroglu, A. E., Preparation and characterization of alumina-supported iron nanoparticles and its application for the removal of aqueous Cu2+ ions. *Chemical Engineering Journal* **2011,** *168* (2), 979-984.

23. Kuang, Y.; Zhou, Y.; Chen, Z. L.; Megharaj, M.; Naidu, R., Impact of Fe and Ni/Fe nanoparticles on biodegradation of phenol by the strain Bacillus fusiformis (BFN) at various pH values. *Bioresource Technology* **2013,** *136*, 588-594.

24. Zhang, X.; Lin, S.; Chen, Z. L.; Megharaj, M.; Naidu, R., Kaolinite-supported nanoscale zero-valent iron for removal of Pb2+ from aqueous solution: Reactivity, characterization and mechanism. *Water Research* **2011,** *45* (11), 3481-3488.

25. Xu, S.; Wang, Z. L., One-dimensional ZnO nanostructures: Solution growth and functional properties. *Nano Research* **2011,** *4* (11), 1013-1098.

26. Guo, J.; Wang, R. Y.; Tjiu, W. W.; Pan, J. S.; Liu, T. X., Synthesis of Fe nanoparticles@graphene composites for environmental applications. *Journal of Hazardous Materials* **2012,** *225*, 63-73.

27. Varis, O.; Vakkilainen, P., China's 8 challenges to water resources management in the first quarter of the 21st Century. *Geomorphology* **2001,** *41* (2-3), 93-104.

28. Diamond, M. L.; de Wit, C. A.; Molander, S.; Scheringer, M.; Backhaus, T.; Lohmann, R.; Arvidsson, R.; Bergman, A.; Hauschild, M.; Holoubek, I.; Persson, L.; Suzuki, N.; Vighi, M.; Zetzsch, C., Exploring the planetary boundary for chemical pollution. *Environment International* **2015,** *78*, 8-15.

29. Godoy, P.; Hewitt, N. J.; Albrecht, U.; Andersen, M. E.; Ansari, N.; Bhattacharya, S.; Bode, J. G.; Bolleyn, J.; Borner, C.; Bottger, J.; Braeuning, A.; Budinsky, R. A.; Burkhardt, B.; Cameron, N. R.; Camussi, G.; Cho, C. S.; Choi, Y. J.; Rowlands, J. C.; Dahmen, U.; Damm, G.; Dirsch, O.; Donato, M. T.; Dong, J.; Dooley, S.; Drasdo, D.; Eakins, R.; Ferreira, K. S.; Fonsato, V.; Fraczek, J.; Gebhardt, R.; Gibson, A.; Glanemann, M.; Goldring, C. E. P.; Gomez-Lechon, M. J.; Groothuis, G. M. M.; Gustavsson, L.; Guyot, C.; Hallifax, D.; Hammad, S.; Hayward, A.; Haussinger, D.; Hellerbrand, C.; Hewitt, P.; Hoehme, S.; Holzhutter, H. G.; Houston, J. B.; Hrach, J.; Ito, K.; Jaeschke, H.; Keitel, V.; Kelm, J. M.; Park, B. K.; Kordes, C.; Kullak-Ublick, G. A.; LeCluyse, E. L.; Lu, P.; Luebke-Wheeler, J.; Lutz, A.; Maltman, D. J.; Matz-Soja, M.; McMullen, P.; Merfort, I.; Messner, S.; Meyer, C.; Mwinyi, J.; Naisbitt, D. J.; Nussler, A. K.; Olinga, P.; Pampaloni, F.; Pi, J. B.; Pluta, L.;

Przyborski, S. A.; Ramachandran, A.; Rogiers, V.; Rowe, C.; Schelcher, C.; Schmich, K.; Schwarz, M.; Singh, B.; Stelzer, E. H. K.; Stieger, B.; Stober, R.; Sugiyama, Y.; Tetta, C.; Thasler, W. E.; Vanhaecke, T.; Vinken, M.; Weiss, T. S.; Widera, A.; Woods, C. G.; Xu, J. J.; Yarborough, K. M.; Hengstler, J. G., Recent advances in 2D and 3D in vitro systems using primary hepatocytes, alternative hepatocyte sources and non-parenchymal liver cells and their use in investigating mechanisms of hepatotoxicity, cell signaling and ADME. *Archives of Toxicology* **2013,** *87* (8), 1315-1530.

30. Anipsitakis, G. P.; Dionysiou, D. D., Degradation of organic contaminants in water with sulfate radicals generated by the conjunction of peroxymonosulfate with cobalt. *Environmental Science & Technology* **2003,** *37* (20), 4790-4797.

31. Peng, J. F.; Song, Y. H.; Yuan, P.; Xiao, S. H.; Han, L., An novel identification method of the environmental risk sources for surface water pollution accidents in chemical industrial parks. *Journal of Environmental Sciences-China* **2013,** *25* (7), 1441-1449.

32. Lu, Y. H.; Xu, S. C.; He, M. D.; Chen, C. H.; Zhang, L.; Liu, C.; Chu, F.; Yu, Z. P.; Zhou, Z.; Zhong, M., Glucose administration attenuates spatial memory deficits induced by chronic low-power-density microwave exposure. *Physiology & Behavior* **2012,** *106* (5), 631-637.

33. Zhao, Y. L.; Yang, L. M.; Wang, Q. Q., Modeling persistent organic pollutant (POP) partitioning between tree bark and air and its application to spatial monitoring of atmospheric POPs in mainland China. *Environmental Science & Technology* **2008,** *42* (16), 6046-6051.

34. Ward, F. A., Economics in integrated water management. *Environmental Modelling & Software* **2009,** *24* (8), 948-958.

35. Burton, D. J.; Yang, Z. Y., FLUORINATED ORGANOMETALLICS - PERFLUOROALKYL AND FUNCTIONALIZED PERFLUOROALKYL

ORGANOMETALLIC REAGENTS IN ORGANIC-SYNTHESIS. *Tetrahedron* **1992,** *48* (2), 189-275.

36. Hutton, G.; Haller, L.; Bartram, J., Global cost-benefit analysis of water supply and sanitation interventions. *Journal of Water and Health* **2007,** *5* (4), 481-502.

37. Qin, H. P.; Su, Q.; Khu, S. T., Assessment of environmental improvement measures using a novel integrated model: A case study of the Shenzhen River catchment, China. *Journal of Environmental Management* **2013,** *114*, 486-495.

38. Wang, S., A comparative study of Fenton and Fenton-like reaction kinetics in decolourisation of wastewater. *Dyes and Pigments* **2008,** *76* (3), 714-720.

39. Brillas, E.; Mur, E.; Sauleda, R.; Sanchez, L.; Peral, J.; Domenech, X.; Casado, J., Aniline mineralization by AOP's: anodic oxidation, photocatalysis, electro-Fenton and photoelectro-Fenton processes. *Applied Catalysis B-Environmental* **1998,** *16* (1), 31-42.

40. Glaze, W. H.; Kang, J. W.; Chapin, D. H., THE CHEMISTRY OF WATER-TREATMENT PROCESSES INVOLVING OZONE, HYDROGEN-PEROXIDE AND ULTRAVIOLET-RADIATION. *Ozone-Science & Engineering* **1987,** *9* (4), 335-352.

41. Davoli, E.; Gangai, M. L.; Morselli, L.; Tonelli, D., Characterisation of odorants emissions from landfills by SPME and GC/MS. *Chemosphere* **2003,** *51* (5), 357-368.

42. Stern, J. C.; Chanton, J.; Abichou, T.; Powelson, D.; Yuan, L.; Escoriza, S.; Bogner, J., Use of a biologically active cover to reduce landfill methane emissions and enhance methane oxidation. *Waste Management* **2007,** *27* (9), 1248-1258.

43. Ito, A.; Takahashi, I.; Nagata, Y.; Chiba, K.; Haraguchi, H., Spatial and temporal characteristics of urban atmospheric methane in Nagoya City, Japan: an assessment of the contribution from regional landfills. *Atmospheric Environment* **2001,** *35* (18), 3137-3144.

44. Kim, K. H.; Choi, Y. J.; Jeon, E. C.; Sunwoo, Y., Characterization of malodorous sulfur compounds in landfill gas. *Atmospheric Environment* **2005,** *39* (6), 1103-1112.

45. Ribeiro, R. S.; Silva, A. M. T.; Pastrana-Martinez, L. M.; Figueiredo, J. L.; Faria, J. L.; Gomes, H. T., Graphene-based materials for the catalytic wet peroxide oxidation of highly concentrated 4-nitrophenol solutions. *Catalysis Today* **2015,** *249*, 204-212.

46. Luck, F., Wet air oxidation: past, present and future. *Catalysis Today* **1999,** *53* (1), 81-91.

47. Levec, J.; Pintar, A., Catalytic wet-air oxidation processes: A review. *Catalysis Today* **2007,** *124* (3-4), 172-184.

48. Akinwande, D., INVERSION OF THE ELECTRICAL AND OPTICAL PROPERTIES OF PARTIALLY OXIDIZED HEXAGONAL BORON NITRIDE. *Nano* **2014,** *9* (1), 27-38.

49. Gogate, P. R.; Mededovic-Thagard, S.; McGuire, D.; Chapas, G.; Blackmon, J.; Cathey, R., Hybrid reactor based on combined cavitation and ozonation: From concept to practical reality. *Ultrasonics Sonochemistry* **2014,** *21* (2), 590-598.

50. Cailean, D.; Teodosiu, C.; Friedl, A., Integrated Sono-Fenton ultrafiltration process for 4-chlorophenol removal from aqueous effluents: assessment of operational parameters (Part 1). *Clean Technologies and Environmental Policy* **2014,** *16* (6), 1145-1160.

51. Nahire, R.; Haldar, M. K.; Paul, S.; Ambre, A. H.; Meghnani, V.; Layek, B.; Katti, K. S.; Gange, K. N.; Singh, J.; Sarkar, K.; Mallik, S., Multifunctional polymersomes for cytosolic delivery of gemcitabine and doxorubicin to cancer cells. *Biomaterials* **2014,** *35* (24), 6482-6497.

52. Nayak, A. P.; Dolocan, A.; Lee, J.; Chang, H.-Y.; Pandhi, T.; Holt, M.; Tao, L.; Akinwande, D., INVERSION OF THE ELECTRICAL AND OPTICAL PROPERTIES OF PARTIALLY OXIDIZED HEXAGONAL BORON NITRIDE. *Nano* **2014,** *9* (1).

53. Lee, O. M.; Kim, H. Y.; Park, W.; Kim, T.-H.; Yu, S., A comparative study of disinfection efficiency and regrowth control of microorganism in secondary wastewater

effluent using UV, ozone, and ionizing irradiation process. *Journal of hazardous materials* **2015,** *295*, 201-8.

54. Packyam, G. S.; Kavitha, S.; Kumar, S. A.; Kaliappan, S.; Yeom, I. T.; Banu, J. R., Effect of sonically induced deflocculation on the efficiency of ozone mediated partial sludge disintegration for improved production of biogas. *Ultrasonics Sonochemistry* **2015,** *26*, 241-248.

55. Petkov, B. H.; Vitale, V.; Mazzola, M.; Lanconelli, C.; Lupi, A., Chaotic behaviour of the short-term variations in ozone column observed in Arctic. *Communications in Nonlinear Science and Numerical Simulation* **2015,** *26* (1-3), 238-249.

56. Predmore, A.; Sanglay, G.; Li, J.; Lee, K., Control of human norovirus surrogates in fresh foods by gaseous ozone and a proposed mechanism of inactivation. *Food Microbiology* **2015,** *50*, 118-125.

57. Sowmya Packyam, G.; Kavitha, S.; Adish Kumar, S.; Kaliappan, S.; Yeom, I. T.; Rajesh Banu, J., Effect of sonically induced deflocculation on the efficiency of ozone mediated partial sludge disintegration for improved production of biogas. *Ultrasonics sonochemistry* **2015,** *26*, 241-8.

58. Wang, W.; Chai, S.; Wang, H.; Fan, W.; Yu, K.; Liang, S.; Ma, J., The Influence of Sulfur Dioxide on Dobson Spectrophotometer Total Ozone Measurement: Analysis on the Basis of Theoretical Factor. *Journal of Coastal Research* **2015**, 353-358.

59. Gupta, S.; Hannah, S.; Watson, C. P.; Sutta, P.; Pedersen, R. H.; Gadegaard, N.; Gleskova, H., Ozone oxidation methods for aluminum oxide formation: Application to low-voltage organic transistors. *Organic Electronics* **2015,** *21*, 132-137.

60. Zhou, H.; Liu, J.; Xia, H.; Zhang, Q.; Ying, T.; Hu, T., Removal and reduction of selected organic micro-pollutants in effluent sewage by the ozone-based oxidation processes. *Chemical Engineering Journal* **2015,** *269*, 245-254.

61. Assumpcao, M. H. M. T.; Piasentin, R. M.; Hammer, P.; De Souza, R. F. B.; Buzzo, G. S.; Santos, M. C.; Spinace, E. V.; Neto, A. O.; Silva, J. C. M., Oxidation of ammonia using PtRh/C electrocatalysts: Fuel cell and electrochemical evaluation. *Applied Catalysis B-Environmental* **2015,** *174*, 136-144.

62. Munoz, F.; Hua, C.; Kwong, T.; Tran, L.; Nguyen, T. Q.; Haan, J. L., Palladium-copper electrocatalyst for the promotion of the electrochemical oxidation of polyalcohol fuels in the alkaline direct alcohol fuel cell. *Applied Catalysis B-Environmental* **2015,** *174*, 323-328.

63. Yang, J.; Wang, Q.; Zhang, M.; Zhang, S.; Zhang, L., An electrochemical fungicide pyrimethanil sensor based on carbon nanotubes/ionic-liquid construction modified electrode. *Food chemistry* **2015,** *187*, 1-6.

64. Zhang, J.; Zhang, L.; Zhang, J.; Zhang, Z.; Wu, Z., Effect of surface/bulk oxygen vacancies on the structure and electrochemical performance of TiO2 nanoparticles. *Journal of Alloys and Compounds* **2015,** *642*, 28-33.

65. Han, H. S.; Yun, M.; Jeong, H.; Jeon, S., Electrocatalytic Oxidation of Formic Acid in an Alkaline Solution with Graphene-Oxide-Supported Ag and Pd Alloy Nanoparticles. *Journal of Nanoscience and Nanotechnology* **2015,** *15* (8), 5699-5705.

66. Jiang, Y.; Liu, X.; Li, J.; Zhou, L.; Yang, X.; Huang, Y., Enhanced Electrochemical Oxidation of p-Nitrophenol Using Single-Walled Carbon Nanotubes/Silver Nanowires Hybrids Modified Electrodes. *Journal of Nanoscience and Nanotechnology* **2015,** *15* (8), 6078-6081.

67. Zhang, X.; Ma, L.-X., Electrochemical fabrication of platinum nanoflakes on fulleropyrrolidine nanosheets and their enhanced electrocatalytic activity and stability for methanol oxidation reaction. *Journal of Power Sources* **2015,** *286*, 400-405.

68. Pi, Y.; Zheng, Z.; Bao, M.; Li, Y.; Zhou, Y.; Sang, G., Treatment of partially hydrolyzed polyacrylamide wastewater by combined Fenton oxidation and anaerobic biological processes. *Chemical Engineering Journal* **2015,** *273*, 1-6.

69. Punzi, M.; Anbalagan, A.; Borner, R. A.; Svensson, B.-M.; Jonstrup, M.; Mattiasson, B., Degradation of a textile azo dye using biological treatment followed by photo-Fenton oxidation: Evaluation of toxicity and microbial community structure. *Chemical Engineering Journal* **2015,** *270*, 290-299.

70. Cui, X.; Zeng, P.; Qiu, G.; Liu, Y.; Song, Y.; Xie, X.; Han, L., Pilot-scale treatment of pharmaceutical berberine wastewater by Fenton oxidation. *Environmental Earth Sciences* **2015,** *73* (9), 4967-4977.

71. Wei, J.; Song, Y.; Meng, X.; Pic, J.-S., Combination of Fenton oxidation and sequencing batch membrane bioreactor for treatment of dry-spun acrylic fiber wastewater. *Environmental Earth Sciences* **2015,** *73* (9), 4911-4921.

72. Zhang, Y.; Zhuang, Y.; Wu, C.; Li, S.; Ma, J., Catalytic Property of Ferryl (IV) Species in the Heterogeneous Thermal Fenton-Like Oxidation System. *Journal of Environmental Engineering* **2015,** *141* (5).

73. Muraza, O.; Galadima, A., Aquathermolysis of heavy oil: A review and perspective on catalyst development. *Fuel* **2015,** *157*, 219-231.

74. Takizawa, S.; Groger, H.; Sasai, H., Vanadium in asymmetric synthesis: emerging concepts in catalyst design and applications. *Chemistry (Weinheim an der Bergstrasse, Germany)* **2015,** *21* (25), 8992-7.

75. Tan, Y. H.; Abdullah, M. O.; Nolasco-Hipolito, C., The potential of waste cooking oil-based biodiesel using heterogeneous catalyst derived from various calcined eggshells coupled with an emulsification technique: A review on the emission reduction and engine performance. *Renewable & Sustainable Energy Reviews* **2015,** *47*, 589-603.

76. Dittmeyer, R.; Grunwaldt, J. D.; Pashkova, A., A review of catalyst performance and novel reaction engineering concepts in direct synthesis of hydrogen peroxide. *Catalysis Today* **2015,** *248*, 149-159.

77. Dange, P. N.; Kulkarni, A. V.; Rathod, V. K., Ultrasound assisted synthesis of methyl butyrate using heterogeneous catalyst. *Ultrasonics Sonochemistry* **2015,** *26*, 257-264.

78. Kaur, M.; Verma, A.; Rajput, H., Potential use of Foundry Sand as Heterogeneous Catalyst in Solar Photo-Fenton Degradation of Herbicide Isoproturon. *International Journal of Environmental Research* **2015,** *9* (1), 85-92.

79. Nasrollahzadeh, M.; Sajadi, S. M.; Rostami-Vartooni, A.; Khalaj, M., Natrolite zeolite supported copper nanoparticles as an efficient heterogeneous catalyst for the 1,3-diploar cycloaddition and cyanation of aryl iodides under ligand-free conditions. *Journal of colloid and interface science* **2015,** *453*, 237-43.

80. Rajput, J. K.; Arora, P.; Kaur, G.; Kaur, M., CuFe2O4 magnetic heterogeneous nanocatalyst: Low power sonochemical-coprecipitation preparation and applications in synthesis of 4H-chromene-3-carbonitrile scaffolds. *Ultrasonics Sonochemistry* **2015,** *26*, 229-240.

81. Sarve, A.; Sonawane, S. S.; Varma, M. N., Ultrasound assisted biodiesel production from sesame (Sesamum indicum L.) oil using barium hydroxide as a heterogeneous catalyst: Comparative assessment of prediction abilities between response surface methodology (RSM) and artificial neural network (ANN). *Ultrasonics Sonochemistry* **2015,** *26*, 218-228.

82. Gurunathan, B.; Ravi, A., Process optimization and kinetics of biodiesel production from neem oil using copper doped zinc oxide heterogeneous nanocatalyst. *Bioresource Technology* **2015,** *190*, 424-428.

83. Ahmad, K.; Alt, H. G., omega-Phenoxyalkyl substituted bis(indenyl) zirconium dichloride complexes as catalysts for homogeneous ethylene polymerization. *Inorganica Chimica Acta* **2015,** *433*, 63-71.

84. Zapico, R. R.; Marin, P.; Diez, F. V.; Ordonez, S., Influence of operation conditions on the copper-catalysed homogeneous wet oxidation of phenol: Development of a kinetic model. *Chemical Engineering Journal* **2015,** *270*, 122-132.

85. Pritchard, J.; Filonenko, G. A.; van Putten, R.; Hensen, E. J. M.; Pidko, E. A., Heterogeneous and homogeneous catalysis for the hydrogenation of carboxylic acid derivatives: history, advances and future directions. *Chemical Society reviews* **2015,** *44* (11), 3808-33.

86. Labus, K.; Szymanska, K.; Bryjak, J.; Jarzebski, A. B., Immobilisation of tyrosinase on siliceous cellular foams affording highly effective and stable biocatalysts. *Chemical Papers* **2015,** *69* (8), 1058-1066.

87. Mutlu, B. R.; Hirschey, K.; Wackett, L. P.; Aksan, A., Long-term preservation of silica gel-encapsulated bacterial biocatalysts by desiccation. *Journal of Sol-Gel Science and Technology* **2015,** *74* (3), 823-833.

88. Faber, K.; Fessner, W.-D.; Turner, N. J., Engineering Biocatalysts for Synthesis Including Cascade Processes. *Advanced Synthesis & Catalysis* **2015,** *357* (8), 1565-1566.

89. Lopez-Gallego, F.; Yate, L., Selective biomineralization of Co-3(PO4)(2)-sponges triggered by His-tagged proteins: efficient heterogeneous biocatalysts for redox processes. *Chemical Communications* **2015,** *51* (42), 8753-8756.

90. Lilienthal, S.; Shpilt, Z.; Wang, F.; Orbach, R.; Willner, I., Programmed DNAzyme-Triggered Dissolution of DNA-Based. Hydrogels: Means for Controlled Release of Biocatalysts and for the Activation of Enzyme Cascades. *Acs Applied Materials & Interfaces* **2015,** *7* (16), 8923-8931.

91. Smith, M. R.; Khera, E.; Wen, F., Engineering Novel and Improved Biocatalysts by Cell Surface Display. *Industrial & Engineering Chemistry Research* **2015,** *54* (16), 4021-4032.

92. Chen, Z.; Ji, H.; Zhao, C.; Ju, E.; Ren, J.; Qu, X., Individual Surface-Engineered Microorganisms as Robust Pickering Interfacial Biocatalysts for Resistance-Minimized Phase-Transfer Bioconversion. *Angewandte Chemie-International Edition* **2015,** *54* (16), 4904-4908.

93. Yang, Y.; Zhang, S.; Wang, S.; Zhang, K.; Wang, H.; Huang, J.; Deng, S.; Wang, B.; Wang, Y.; Yu, G., Ball Milling Synthesized MnOx as Highly Active Catalyst for Gaseous POPs Removal: Significance of Mechanochemically Induced Oxygen Vacancies. *Environmental Science & Technology* **2015,** *49* (7), 4473-4480.

94. Sun, Y.; Zhang, X., Analysis of Transient Conduction and Radiation Problems Using the Lattice Boltzmann and Discrete Ordinates Methods. *Numerical Heat Transfer Part a-Applications* **2015,** *68* (6), 619-637.

95. Michalik-Zym, A.; Dula, R.; Duraczynska, D.; Krysciak-Czerwenka, J.; Machej, T.; Socha, R. P.; Wlodarczyk, W.; Gawel, A.; Matusik, J.; Bahranowski, K.; Wisla-Walsh, E.; Litynska-Dobrzynska, L.; Serwicka, E. M., Active, selective and robust Pd and/or Cr catalysts supported on Ti-, Zr- or Ti,Zr -pillared montmorillonites for destruction of chlorinated volatile organic compounds. *Applied Catalysis B-Environmental* **2015,** *174*, 293-307.

96. Shahidi, D.; Roy, R.; Azzouz, A., Advances in catalytic oxidation of organic pollutants - Prospects for thorough mineralization by natural clay catalysts. *Applied Catalysis B-Environmental* **2015,** *174*, 277-292.

97. Zhang, D.; Cheng, T.; Liu, G., An imidazolium-based organopalladium-functionalized organic-inorganic hybrid silica promotes one-pot tandem Suzuki cross

coupling-reduction of haloacetophenones and arylboronic acids. *Applied Catalysis B-Environmental* **2015,** *174*, 344-349.

98. Ford, T. A., The molecular complexes of boron trifluoride with nitrosyl fluoride and nitrosyl chloride. Ion-pair formation. *Journal of Molecular Structure* **2015,** *1090*, 7-13.

99. Ben Hammouda, S.; Adhoum, N.; Monser, L., Synthesis of magnetic alginate beads based on Fe3O4 nanoparticles for the removal of 3-methylindole from aqueous solution using Fenton process. *Journal of Hazardous Materials* **2015,** *294*, 128-136.

100. Hammouda, S. B.; Adhoum, N.; Monser, L., Synthesis of magnetic alginate beads based on Fe3O4 nanoparticles for the removal of 3-methylindole from aqueous solution using Fenton process. *Journal of hazardous materials* **2015,** *294*, 128-36.

101. Fang, Q.; Cheng, Q.; Xu, H.; Xuan, S., Monodisperse magnetic core/shell microspheres with Pd nanoparticles-incorporated-carbon shells. *Dalton Transactions* **2014,** *43* (6), 2588-2595.

102. Park, H. H.; Woo, K.; Ahn, J.-P., Core-Shell Bimetallic Nanoparticles Robustly Fixed on the Outermost Surface of Magnetic Silica Microspheres. *Scientific Reports* **2013,** *3*.

103. Guo, H.; Liu, X.; Hou, Y.; Xie, Q.; Wang, L.; Geng, H.; Peng, D.-L., Magnetically separable and recyclable urchin-like Co-P hollow nanocomposites for catalytic hydrogen generation. *Journal of Power Sources* **2014,** *260*, 100-108.

104. Kumar, P.; Gill, K.; Kumar, S.; Ganguly, S. K.; Jain, S. L., Magnetic Fe3O4@MgAl-LDH composite grafted with cobalt phthalocyanine as an efficient heterogeneous catalyst for the oxidation of mercaptans. *Journal of Molecular Catalysis a-Chemical* **2015,** *401*, 48-54.

105. Nikoorazm, M.; Ghorbani-Choghamarani, A.; Mandavi, H.; Esmaeili, S. M., Efficient oxidative coupling of thiols and oxidation of sulfides using UHP in the presence of Ni or Cd salen complexes immobilized on MCM-41 mesoporous as novel and recoverable nanocatalysts. *Microporous and Mesoporous Materials* **2015,** *211*, 174-181.

106. Rostami, A.; Tahmasbi, B.; Abedi, F.; Shokri, Z., Magnetic nanoparticle immobilized N-propylsulfamic acid: The chemoselective, efficient, green and reusable nanocatalyst for oxidation of sulfides to sulfoxides using H2O2 under solvent-free conditions. *Journal of Molecular Catalysis a-Chemical* **2013,** *378*, 200-205.

107. Safavi, A.; Momeni, S., Highly efficient degradation of azo dyes by palladium/hydroxyapatite/Fe3O4 nanocatalyst. *Journal of Hazardous Materials* **2012,** *201*, 125-131.

108. Selvaraju, T.; Das, J.; Han, S. W.; Yang, H., Ultrasensitive electrochemical immunosensing using magnetic beads and gold nanocatalysts. *Biosensors & Bioelectronics* **2008,** *23* (7), 932-938.

109. Wang, S.; Zhang, Z.; Liu, B., Catalytic Conversion of Fructose and 5-Hydroxymethylfurfural into 2,5-Furandicarboxylic Acid over a Recyclable Fe3O4-CoOx Magnetite Nanocatalyst. *Acs Sustainable Chemistry & Engineering* **2015,** *3* (3), 406-412.

110. Hu, L.; Lin, L.; Wu, Z.; Zhou, S.; Liu, S., Chemocatalytic hydrolysis of cellulose into glucose over solid acid catalysts. *Applied Catalysis B-Environmental* **2015,** *174*, 225-243.

111. Jing, H.; Wang, X.; Liu, Y.; Wang, A., Preparation of magnetic nanocomposites of solid acid catalysts and their applicability in esterification. *Chinese Journal of Catalysis* **2015,** *36* (2), 244-251.

112. (a) Li, R.; Jia, Y.; Bu, N.; Wu, J.; Zhen, Q., Photocatalytic degradation of methyl blue using Fe2O3/TiO2 composite ceramics. *Journal of Alloys and Compounds* **2015,** *643*, 88-93; (b) Li, Y.; Zhao, M.; Zhang, N.; Li, R.; Chen, J., Synthesis and photocatalytic activity of carbon spheres loaded Cu2O/Cu composites. *Journal of Alloys and Compounds* **2015,** *643*, 106-110; (c) Shirsath, D. S.; Shrivastava, V. S., Photocatalytic Removal of O- Nitro Phenol from Wastewater by Novel an Eco-friendly Magnetic Nanoadsorbent. *International Journal of Environmental Research* **2015,** *9* (1), 363-372; (d) Yin, H.; Dai, X.; Zhu, M.; Li, F.; Feng,

X.; Liu, F., Fe-doped cryptomelane synthesized by refluxing at atmosphere: Structure, properties and photocatalytic degradation of phenol. *Journal of hazardous materials* **2015,** *296*, 221-9.

113. Yu, L.; Yang, X.; Wang, D., TiO_2 incorporated in magnetic mesoporous SBA-15 by a facile inner-pore hydrolysis process toward enhanced adsorption-photocatalysis performances for As(III). *Journal of colloid and interface science* **2015,** *448*, 525-32.

114. Ambashta, R. D.; Bhatnagar, A.; Sillanpaa, M. E. T., Supported iron-based catalysts under influence of static magnetic field for the removal of TBP and EDTA. *Desalination and Water Treatment* **2015,** *54* (10), 2700-2709.

115. Atashkar, B.; Rostami, A.; Gholami, H.; Tahmasbi, B., Magnetic nanoparticles Fe3O4-supported guanidine as an efficient nanocatalyst for the synthesis of 2H-indazolo 2,1-b phthalazine-triones under solvent-free conditions. *Research on Chemical Intermediates* **2015,** *41* (6), 3675-3681.

116. Padervand, M.; Vossoughi, M.; Janfada, B., A novel efficient magnetic core-zeolitic shell nanocatalyst system: preparation, characterization and activity. *Chemical Papers* **2015,** *69* (6), 856-863.

117. Shaabani, A.; Nosrati, H.; Seyyedhamzeh, M., Cellulose@Fe2O3 nanoparticle composites: magnetically recyclable nanocatalyst for the synthesis of 3-aminoimidazo 1,2-a pyridines. *Research on Chemical Intermediates* **2015,** *41* (6), 3719-3727.

3 Synthesis of magnetic carbon nanosphere supported manganese catalysts with a one-pot hydrothermal method

A B S T R A C T

Magnetic carbon nanospheres supported Mn nanoparticles were synthesized by a one-pot hydrothermal method with the carbon supplied by glucose. The samples were characterized by field emission scanning electron microscopy (FE-SEM), X-Ray diffraction (XRD), thermogravimetric analysis/differential temperature gradient (TGA/DTG) and Fourier transform infrared spectrscopy (FT-IR). The catalysts were evaluated for phenol degradation, which could be effectively decomposed in 180 minutes.

3.1 Introduction

Due to the increasingly faster pace of global industrialization and people's lacking of awareness of environmental protection, water and soil contamination has become a critical issue worldwide[1]. The contaminated sites not only reduce the availability of fertile land for agricultural use but also pose a risk to public health, food system and ground water[2]. Among the pollutants discharged from industrial sites, contaminants of persistent organic pollutants (POPs) have attracted particular concern owing to their long life-time[3], toxicity[4] and resistance[5] against natural attenuation. In recent years, advanced oxidation processes (AOPs) have been proved to be useful for their ability of complete degradation of the POPs[6]. Among AOPs, Fenton system has proved to be an effective one because of its low cost[7] and toxicity[8]. However, it also suffers from some drawbacks, such as high cost[9] and it tends to form aggregates[10].

Hausmannite (Mn_3O_4) has drawn particular research attention because of its distinctive structure[11] and physicochemical properties[8], which are of great interest in energy conversion, magnetics, and catalysis[12]. Despite the high catalytic performance of Mn_3O_4 nanoparticles (NPs), its poor chemical[13] and thermal stabilities[14], which could lead to aggregation of NPs, not only decrease the catalytic efficiency but limits its wider application[15]. To solve this problem, carbonaceous materials with high electrical conductivity and buffer matrix have been widely employed as supports for Mn_3O_4-based catalysts to improve their conductivity and stability[16]. Besides hausmannite, the other form of manganese oxide-MnO_2 also shows its potential as a catalyst in wastewater treatment[17]. Previously, MnO_2 was usually used for the Fenton-like reaction for production of hydroxyl radicals from H_2O_2 and oxidation of organic compounds[8, 18]. Anipsitakis and Dionysiou[19] studied nine transition metal ions for the activation of three oxidants and the generation of sulfate, peroxymonosulfate, and hydroxyl

radicals. They suggested that the conjunction of Mn^{2+} ions were capable of generation of sulfate radicals by activation of peroxymonosulfate. However, the nanosized manganese oxides can bring secondary contamination to water which can be more critical than persistent organic pollutants if the oxides are not being well recovered[14]. To solve this problem, Fe_3O_4/C nanoparticles have attracted huge attention for their special unique magnetic reaction, low toxicity and high modifiable surface[20].

In this chapter, a unique synthesis of magnetic carbon nanospheres supported by Mn catalysts with a one-pot hydrothermal method will be presented. The prepared catalysts showed high activity and good magnetic performance in the reaction of oxidizing phenol solutions.

3.2 Experimental

3.2.1 Chemicals

Iron (II) chloride tetrahydrate, iron (III) hexahydrate (99.9%), potassium permanganate (99.8%), D-glucose (99.9%) and ammonia solution (28%) were purchased from Sigma – Aldrich. Hydrochloric acid (37%) was received from Fluka. High purity nitrogen gas (99.999%) was obtained from BOC. All chemicals mentioned above were used as received without any further purification.

3.2.2 Synthesis of magnetic carbon nanospheres (MCS-one)

In a modified hydrothermal method to synthesize magnetic carbon nanospheres, firstly, 0.02 mol iron (III) hexahydrate (99.9%), 0.01mol iron (II) chloride tetrahydrate and 0.02 mol D-glucose were dissolved in 50 mL ultrapure water, followed by 25 minutes stirring with a magnetic rotor. Secondly, nitrogen bubbling was performed (40 mL/min) in 10 minutes, 28% ammonia solution was added with a rate of 1 mL/min to make solution pH=10 for synthesis of magnetic nanoparticles. Thirdly, nitrogen bubbling was continued for 20 minutes with

stirring and then the solution was transferred into a Teflon-lined autoclave (120 mL) and put in an oven at 160 ℃ for 18h. After cooled down to room temperature, the resultant was filtered and washed by ethanol for three times. Finally, the precipitate was put in the oven at 60 ℃ for 12h for drying. The final sample was named as MCS-one.

3.2.3 Synthesis of MCS supported Mn catalysts (Mn/MCS-one)

In a typical procedure, firstly, 0.25 g MCS-one was dissolved in 50 mL ultrapure water, followed by 10 min sonicating. Secondly, 0.5 g potassium permanganate was added into the above solution and stirred for 10 minutes. Thirdly, 1 ml hydrochloric acid (37%) was added to the above mixture solution and stirred for 20 minutes. After that, the solution was transferred into a Teflon-lined autoclave (120 mL) and put in an oven at 50 ℃. After cool down to room temperature, the resultants were filtered and washed by ethanol for three times. Finally, the precipitates were put in the oven at 60 ℃ for 12h. The final sample was named as Mn/MCS-one.

3.2.4 Characterization of materials

Several techniques were used to identify the physicochemical properties of previous samples. The field emission scanning electron microscopy (FE-SEM, Zeiss Neon 40EsB） was used to test its morphological, size and texture information. The X-ray diffraction (XRD) was used to study crystallographic structures. The XRD was obtained using a Bruker D8-Advance X-Ray diffractometer with Cu Kα radiation (λ = 1.5418 Å) operated at 40 kV and 30 mA, respectively. The thermogravimetric analysis/differential temperature gradient (TGA/DTG) was used to test the manganese content and thermal stability of Mn/MCS-one. The TGA/DTG was carried out on a TGA/DSC 1 instrument of Mettler-Toledo under an air flow at a heating rate of 10 ℃/min. The Fourier transform infrared spectroscopy (FT-IR) analysis was performed on a Perkin-Elmer Model FTIR-100 with a MIR detector.

3.2.5 Catalytic oxidation of phenol solutions

The activeness of the samples was investigated by oxidation of phenol solutions. The batch experiments were carried out in a 250 mL conical flask which contained 20 ppm phenol solution. The conical flask was put in a water bath at temperature of 25 ℃. Firstly, 0.04 g Mn/MCS-one catalysts were added to the phenol solution, after stirring for one minute until adsorption-desorption equilibrium on the catalyst was achieved. 0.4 g of oxone was added to the previously mixed solution to activate the reaction. The reaction kept running for 180 minutes. At predetermined time intervals, 1 mL sample was withdrawn with a syringe and filtered into a high performance liquid chromatography (HPLC) vial, after that, 0.5 mL of methanol was added into the vial to quench the reaction. The water samples were analyzed with a high performance liquid chromatography (HPLC), whose UV detector was set at a wavelength of 270 nm. The mobile phase was made with 30% CH_3CN and 70% deionized water and the flow rate was 1 mL/min. In order to evaluate the catalysts' ability, the annealed catalysts were recycled with magnetic field and washed with ultrapure water for three times.

3.3 Results and discussion

3.3.1 Characterization of the composites

Fig.3.1 shows SEM images, which demonstrate the morphology and composition of the Mn/MCS-one. The size of the nanoparticle is around 20 nm. Mn particles were expected to homogeneously distribute on the spheres.

Fig.3.2 shows TGA results, which can determine the content of each element in the hybrids. The test was acted in air with a heating rate of 10 ℃/min. There are two weight loss procedures. It presents a huge step/peak in the range from about 50 to 150℃ for the TG/DTG curves. It can be assigned to the evaporation of adsorbed water elements[21]. A slight weight

loss occurred between 150 to 550℃ which can be assigned to the decomposition of carbon skeleton for the carbon coated on Fe_3O_4[22]. There was no more weight loss after 560℃.

Fig.3.3 shows FT-IR results which are used to analyse the functional groups on the Mn/MCS-one. The bands at 3449, 1669, 1381, 579 cm^{-1} were assigned to –OH, C=O, C-C and Fe-O, respectively.

Fig.3.4 shows N_2 adsorption-desorption isotherms and Fig.3.5 shows the pore size distributions of the Mn/MCS-one. The hysteresis loops in P/P_0 = 0.43-0.98 indicated the mesoporous structure of the sample. Furthermore, the appearance of the H2-type hysteresis loop suggested a porous material with relatively high uniform channel like pores[23]. The specific surface area, pore volume and pore size were 342 m^2/g, 0.266 cm^3/g and 3.1nm, respectively.

Fig.3.6 shows XRD of the crystalline structure of the final samples. The results demonstrate the diffraction peaks at 2θ=30.1°, 35.4°, 43.05°, 56.92° and 62.51°, which present the crystal lanes Fe_3O_4 (220), (311), (400), (422) and (440), respectively. Peaks in Mn/MCS-one were consistent with the standard XRD data for the inverse spinel structure Fe_3O_4 with lattice constants of a = 8.397 Å (JCPDS No.65-3107)[24]. The Fe_3O_4 nanoparticles' average grain size was 20 nm calculated with the Scherrer's formula[25]. On the other hand, the peaks of Mn were too weak to recognise for the reason of low Mn level.

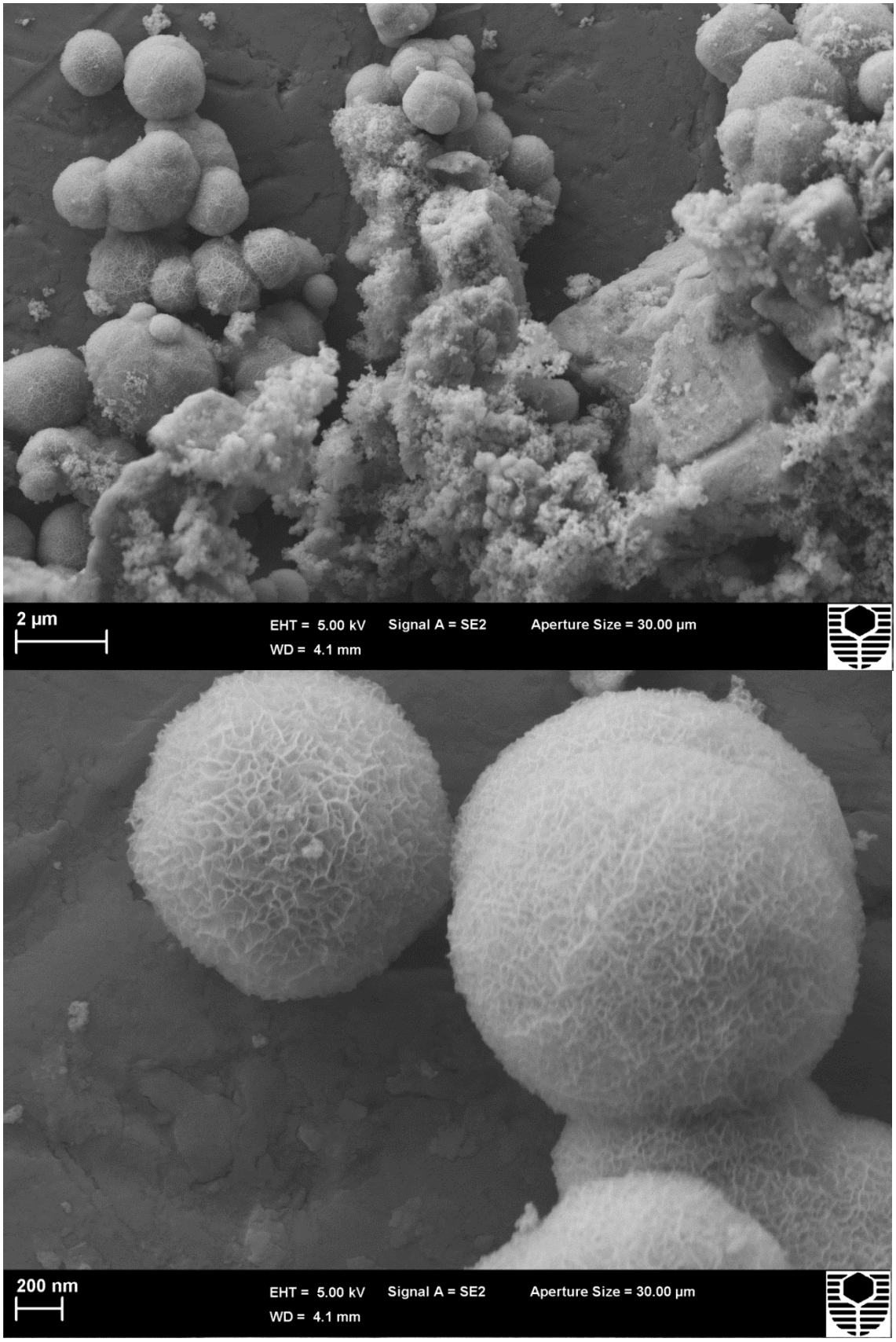

Fig.3.1. SEM images of Mn/MCS-one.

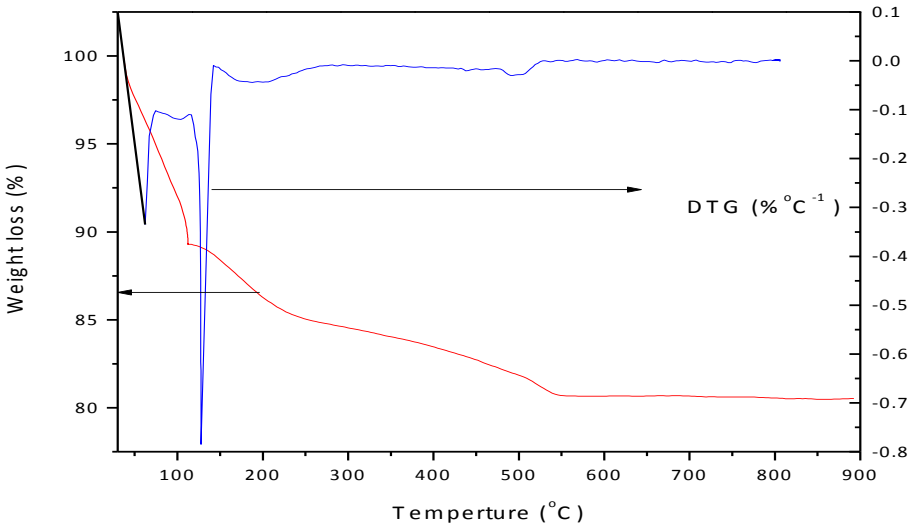

Fig.3.2. TGA and DTG curves of Mn/MCS-one.

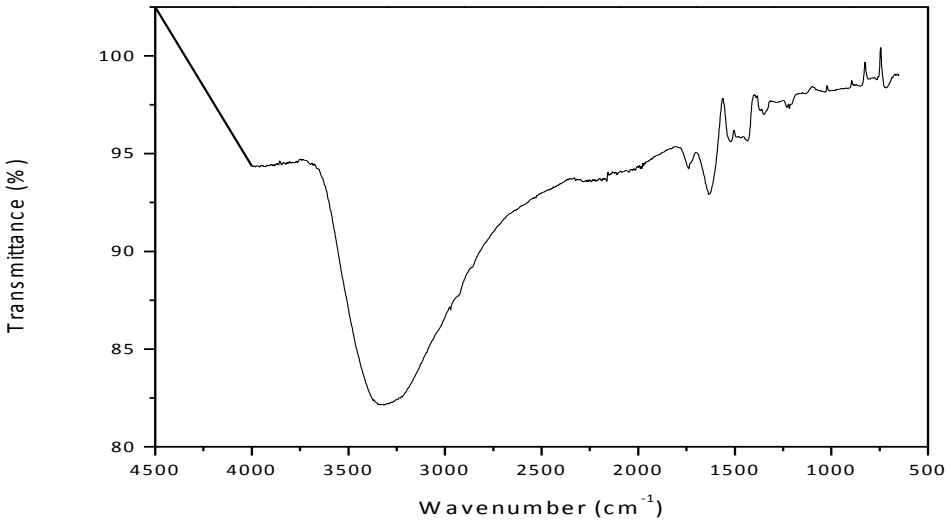

Fig.3.3. FT-IR spectra of Mn/MCS-one.

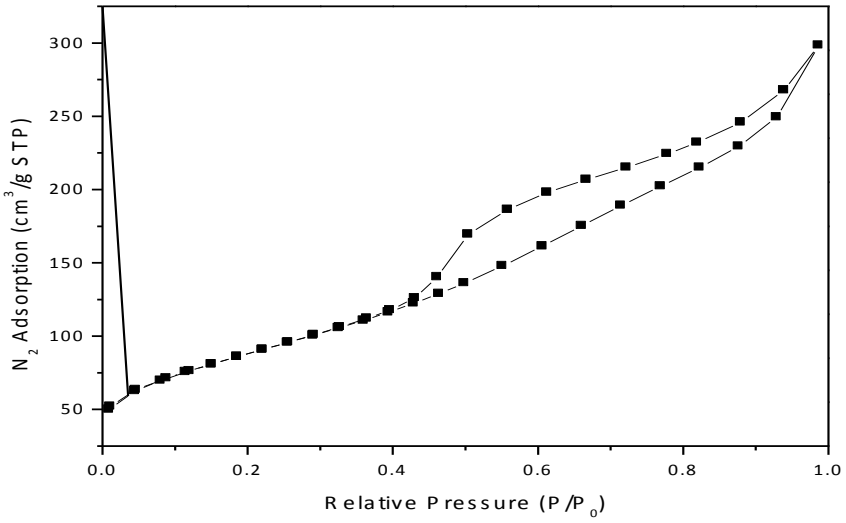

Fig.3.4. N_2 sorption isotherms of Mn/MCS-one.

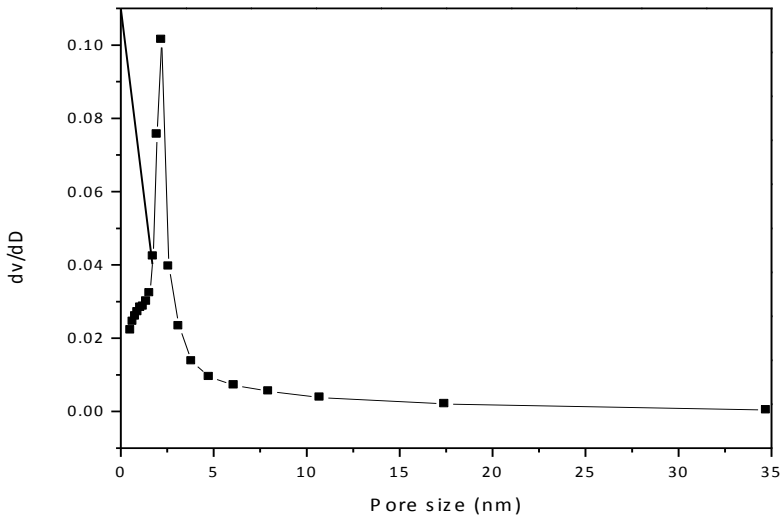

Fig.3.5. Pore size distributions of Mn/MCS-one.

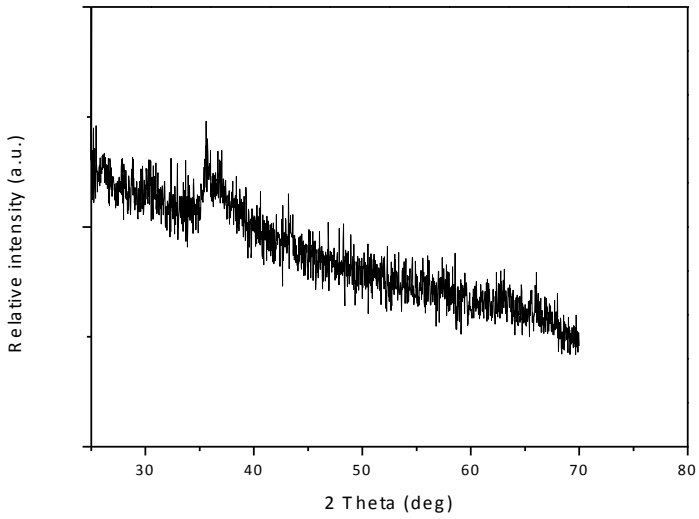

Fig.3.6. XRD patterns of Mn/MCS-one.

3.3.2 Adsorption and heterogeneous phenol degradation

The catalytic oxidation of phenol solutions was carried out and the results are shown in Fig.3.7, which demonstrates the phenol decomposition at different conditions. For the reaction without a catalyst, the final phenol removal rate was about 2% in 180 minutes, which demonstrates PMS itself in homogeneous solution could not induce phenol oxidation. For the adsorption reaction using Mn/MCS-one only, the final phenol removal rate was about 3% in 180 minutes, suggesting that phenol adsorption on Mn/MCS-one is negligible. For the MCS-one loading with PMS for phenol degradation, the final phenol removal rate is about 17% in 180 minutes and for the Mn/MCS-one, the final phenol removal rate can reach nearly 100% in about 180 minutes, suggesting that MCS using as a carrier of manganese oxide will make a more significant contribution to phenol degradation.

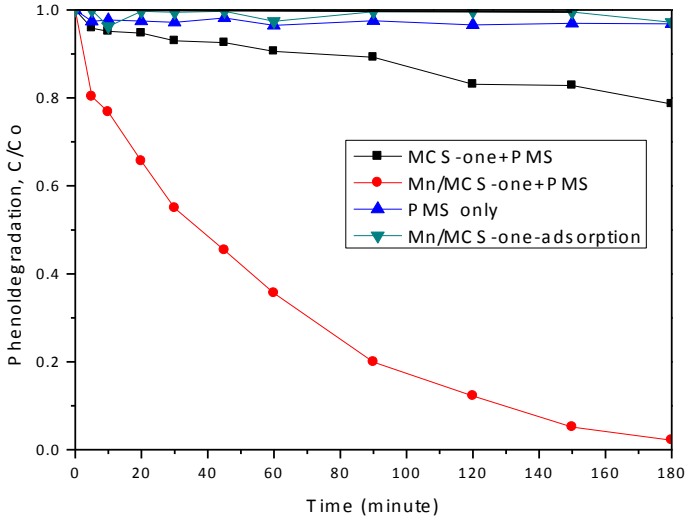

Fig.3.7. Control experiments for phenol removal in different conditions.

3.3.2 Effects of reaction parameters on phenol degradation and stability of the catalysts

In heterogeneous catalytic oxidation of phenol, a lot of conditions can influence the final phenol degradation rate to different extents. This section will show some results of the reaction temperature' effect on phenol degradation.

Fig.3.8 shows the performance of Mn/MCS-one catalysts for heterogeneous oxidation of phenol at varying temperatures. It is seen that reaction temperature dramatically affected oxidation efficiency and degradation rate. When reaction took place at 25 ℃, 35 ℃ and 45 ℃, phenol removal rate can reach to 100% in 180 minutes, 90 minutes and 60 minutes, respectively, suggesting that higher temperature can make a more significant contribution to phenol degradation. Based on reaction rate at different temperatures, the apparent activation energy of Mn/MCS-one was calculated as 12.6 kJ/mol.

It is known that the stability of the catalysts is very important in practical application. Fig.3.9 shows the stability of the Mn/MCS-one catalysts. In the second time, the phenol degradation rate was 80% in 180 minutes, while in the third run; the phenol degradation rate was 60% in 180 minutes, suggesting that the catalytic activities decreased in recycled tests. The decrease in catalytic activity might be attributed to the attachment of reaction intermediates on the catalyst surface which deactivates the correspondent active sites.

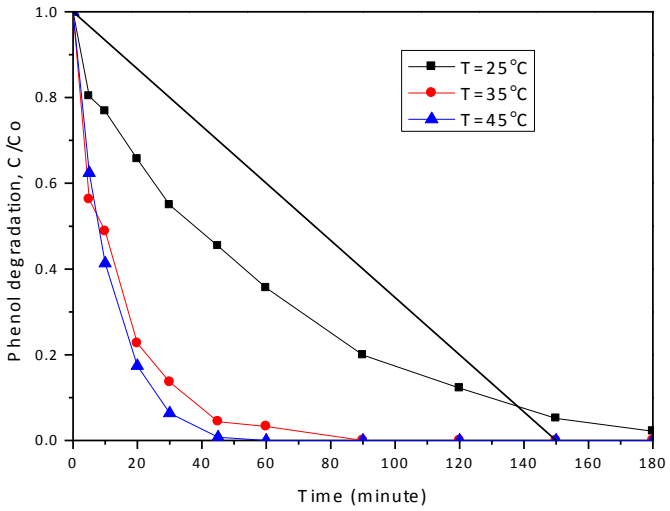

Fig.3.8. Phenol removal at different temperatures.

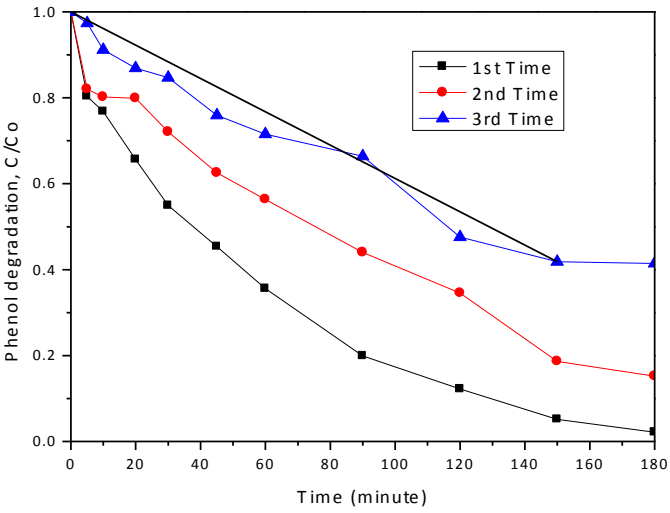

Fig.3.9. Reusability tests of Mn/MCS-one catalyst.

3.4 Summary

The one-pot hydrothermal method has been successfully adopted to synthesize magnetic nanocatalysts. The catalysts demonstrated to be effective for activation of PMS in producing oxidative radicals for degradation of phenol. The apparent activation energy of Mn/MCS-one was calculated as 12.6 kJ/mol. This chapter provided a feasible approach for removal of organic pollutants by magnetically separable catalysts via advanced material design.

3.5 References

1. Nasrabadi, T., An Index Approach to Metallic Pollution in River Waters. *International Journal of Environmental Research* **2015,** *9* (1), 385-394.

2. (a) Brooks, S. J.; Harman, C.; Hultman, M. T.; Berge, J. A., Integrated biomarker assessment of the effects of tailing discharges from an iron ore mine using blue mussels (Mytilus spp.). *Science of the Total Environment* **2015,** *524*, 104-114; (b) Namvar, A.; Khandan, T., Inoculation of rapeseed under different rates of inorganic nitrogen and sulfur fertilizer: impact on water relations, cell membrane stability, chlorophyll content and yield. *Archives of Agronomy and Soil Science* **2015,** *61* (8), 1137-1149.

3. Balmer, B. C.; Ylitalo, G. M.; McGeorge, L. E.; Baugh, K. A.; Boyd, D.; Mullin, K. D.; Rosel, P. E.; Sinclair, C.; Wells, R. S.; Zolman, E. S.; Schwacke, L. H., Persistent organic pollutants (POPs) in blubber of common bottlenose dolphins (Tursiops truncatus) along the northern Gulf of Mexico coast, USA. *Science of the Total Environment* **2015,** *527*, 306-312.

4. Elliott, J. E.; Brogan, J.; Lee, S. L.; Drouillard, K. G.; Elliott, K. H., PBDEs and other POPs in urban birds of prey partly explained by trophic level and carbon source. *Science of the Total Environment* **2015,** *524*, 157-165.

5. Zhang, H.; Bayen, S.; Kelly, B. C., Multi-residue analysis of legacy POPs and emerging organic contaminants in Singapore's coastal waters using gas chromatography-triple quadrupole tandem mass spectrometry. *Science of the Total Environment* **2015,** *523*, 219-232.

6. (a) Barazesh, J. M.; Hennebel, T.; Jasper, J. T.; Sedlak, D. L., Modular Advanced Oxidation Process Enabled by Cathodic Hydrogen Peroxide Production. *Environmental Science & Technology* **2015,** *49* (12), 7391-7399; (b) Wang, D.; Bolton, J. R.; Andrews, S. A.; Hofmann, R., UV/chlorine control of drinking water taste and odour at pilot and full-scale.

Chemosphere **2015,** *136*, 239-44; (c) Zhou, J.; Xiao, J.; Xiao, D.; Guo, Y.; Fang, C.; Lou, X.; Wang, Z.; Liu, J., Transformations of chloro and nitro groups during the peroxymonosulfate-based oxidation of 4-chloro-2-nitrophenol. *Chemosphere* **2015,** *134*, 446-451.

7. Doumic, L. I.; Soares, P. A.; Ayude, M. A.; Cassanello, M.; Boaventura, R. A. R.; Vilar, V. J. P., Enhancement of a solar photo-Fenton reaction by using ferrioxalate complexes for the treatment of a synthetic cotton-textile dyeing wastewater. *Chemical Engineering Journal* **2015,** *277*, 86-96.

8. Yao, Y.; Cai, Y.; Wu, G.; Wei, F.; Li, X.; Chen, H.; Wang, S., Sulfate radicals induced from peroxymonosulfate by cobalt manganese oxides (CoxMn3-xO4) for Fenton-Like reaction in water. *Journal of hazardous materials* **2015,** *296*, 128-37.

9. Qian, W.; Zhang, J.; Xiong, Y.; Chen, X.; Tian, S.; Kong, L.; Guo, Y., Construction and performance of a novel integrative Fenton-like and upward flow biological filter bed. *Chemical Engineering Journal* **2015,** *273*, 166-172.

10. Yang, S.; Yang, L.; Liu, X.; Xie, J.; Zhang, X.; Yu, B.; Wu, R.; Li, H.; Chen, L.; Liu, J., TiO2-doped Fe3O4 nanoparticles as high-performance Fenton-like catalyst for dye decoloration. *Science China-Technological Sciences* **2015,** *58* (5), 858-863.

11. Xu, X.; Yang, J.; Zhao, X.; Zhang, X.; Li, R., Molecular binding mechanisms of manganese to the root cell wall of Phytolacca americana L. using multiple spectroscopic techniques. *Journal of hazardous materials* **2015,** *296*, 185-91.

12. (a) Ledezma, P.; Donose, B. C.; Freguia, S.; Keller, J., Oxidised stainless steel: a very effective electrode material for microbial fuel cell bioanodes but at high risk of corrosion. *Electrochimica Acta* **2015,** *158*, 356-360; (b) Oschmann, B.; Tahir, M. N.; Mueller, F.; Bresser, D.; Lieberwirth, I.; Tremel, W.; Passerini, S.; Zentel, R., Precursor Polymers for the Carbon Coating of Au@ZnO Multipods for Application as Active Material in Lithium-Ion Batteries. *Macromolecular Rapid Communications* **2015,** *36* (11), 1075-1082.

13. Salunkhe, R. R.; Ahn, H.; Kim, J. H.; Yamauchi, Y., Rational design of coaxial structured carbon nanotube-manganese oxide (CNT-MnO2) for energy storage application. *Nanotechnology* **2015,** *26* (20).

14. Sui, Z.-Y.; Wang, C.; Shu, K.; Yang, Q.-S.; Ge, Y.; Wallace, G. G.; Han, B.-H., Manganese dioxide-anchored three-dimensional nitrogen-doped graphene hybrid aerogels as excellent anode materials for lithium ion batteries. *Journal of Materials Chemistry A* **2015,** *3* (19), 10403-10412.

15. Zhu, H.-J.; Zhai, W.; Yang, M.; Liu, X.-m.; Chen, Y.-C.; Yang, H.; Shen, X.-d., Synthesis and characterization of LiMnPO4/C nano-composites from manganese(II) phosphate trihydrate precipitated from a micro-channel reactor approach. *Rsc Advances* **2014,** *4* (49), 25625-25632.

16. Anipsitakis, G. P.; Dionysiou, D. D., Degradation of organic contaminants in water with sulfate radicals generated by the conjunction of peroxymonosulfate with cobalt. *Environmental Science & Technology* **2003,** *37* (20), 4790-4797.

17. (a) Furgal, K. M.; Meyer, R. L.; Bester, K., Removing selected steroid hormones, biocides and pharmaceuticals from water by means of biogenic manganese oxide nanoparticles in situ at ppb levels. *Chemosphere* **2015,** *136*, 321-6; (b) Lee, K.; Ahmed, M. S.; Jeon, S., Electrochemical deposition of silver on manganese dioxide coated reduced graphene oxide for enhanced oxygen reduction reaction. *Journal of Power Sources* **2015,** *288*, 261-269; (c) Simoes, M.; Surace, Y.; Yoon, S.; Battaglia, C.; Pokrant, S.; Weidenkaff, A., Hydrothermal vanadium manganese oxides: Anode and cathode materials for lithium-ion batteries. *Journal of Power Sources* **2015,** *291*, 66-74.

18. Liang, X.; He, Z.; Wei, G.; Liu, P.; Zhong, Y.; Tan, W.; Du, P.; Zhu, J.; He, H.; Zhang, J., The distinct effects of Mn substitution on the reactivity of magnetite in

heterogeneous Fenton reaction and Pb(II) adsorption. *Journal of Colloid and Interface Science* **2014,** *426*, 181-189.

19. Anipsitakis, G. P.; Dionysiou, D. D.; Gonzalez, M. A., Cobalt-mediated activation of peroxymonosulfate and sulfate radical attack on phenolic compounds. Implications of chloride ions. *Environmental Science & Technology* **2006,** *40* (3), 1000-1007.

20. (a) Duan, X.; Sun, H.; Wang, Y.; Kang, J.; Wang, S., N-Doping-Induced Nonradical Reaction on Single-Walled Carbon Nanotubes for Catalytic Phenol Oxidation. *Acs Catalysis* **2015,** *5* (2), 553-559; (b) Wang, Y.; Indrawirawan, S.; Duan, X.; Sun, H.; Ang, H. M.; Tade, M. O.; Wang, S., New insights into heterogeneous generation and evolution processes of sulfate radicals for phenol degradation over one-dimensional alpha-MnO2 nanostructures. *Chemical Engineering Journal* **2015,** *266*, 12-20; (c) Wang, Y.; Sun, H.; Ang, H. M.; Tade, M. O.; Wang, S., Facile Synthesis of Hierarchically Structured Magnetic MnO2/ZnFe2O4 Hybrid Materials and Their Performance in Heterogeneous Activation of Peroxymonosulfate. *Acs Applied Materials & Interfaces* **2014,** *6* (22), 19914-19923; (d) Wang, Y.; Sun, H.; Ang, H. M.; Tade, M. O.; Wang, S., 3D-hierarchically structured MnO2 for catalytic oxidation of phenol solutions by activation of peroxymonosulfate: Structure dependence and mechanism. *Applied Catalysis B-Environmental* **2015,** *164*, 159-167; (e) Wang, Y.; Sun, H.; Duan, X.; Ang, H. M.; Tade, M. O.; Wang, S., A new magnetic nano zero-valent iron encapsulated in carbon spheres for oxidative degradation of phenol. *Applied Catalysis B-Environmental* **2015,** *172*, 73-81; (f) Ye, N.; Li, J.; Wang, Y.; Ma, J., DETERMINATION OF CATECHINS IN TEA BY MICELLAR ELECTROKINETIC CHROMATOGRAPHY WITH A GRAPHENE OXIDE-COATED CAPILLARY. *Instrumentation Science & Technology* **2014,** *42* (6), 605-617.

21. Wang, Y.; Sun, H.; Ang, H. M.; Tade, M. O.; Wang, S., Synthesis of magnetic core/shell carbon nanosphere supported manganese catalysts for oxidation of organics in water by peroxymonosulfate. *Journal of Colloid and Interface Science* **2014,** *433*, 68-75.

22. Yan, Z.; Cai, Y.; Zhu, G.; Yuan, J.; Tu, L.; Chen, C.; Yao, S., Synthesis of 3-fluorobenzoyl chloride functionalized magnetic sorbent for highly efficient enrichment of perfluorinated compounds from river water samples. *Journal of Chromatography A* **2013,** *1321*, 21-29.

23. Kruk, M.; Jaroniec, M., Gas adsorption characterization of ordered organic-inorganic nanocomposite materials. *Chemistry of Materials* **2001,** *13* (10), 3169-3183.

24. Kaur, B.; Tumma, M.; Srivastava, R., Transition-Metal-Exchanged Nanocrystalline ZSM-5 and Metal-Oxide-Incorporated SBA-15 Catalyzed Reduction of Nitroaromatics. *Industrial & Engineering Chemistry Research* **2013,** *52* (33), 11479-11487.

25. Baby, T. T.; Ramaprabhu, S., SiO2 coated Fe3O4 magnetic nanoparticle dispersed multiwalled carbon nanotubes based amperometric glucose biosensor. *Talanta* **2010,** *80* (5), 2016-2022.

4 Synthesis of magnetic carbon nanosphere supported manganese catalysts for phenol degradation

A B S T R A C T

Magnetic carbon nanospheres supported Mn nanoparticles were synthesized by a two-step method with the carbon supplied by glucose. The samples were characterized by field emission scanning electron microscopy (FE-SEM), X-Ray diffraction (XRD), thermogravimetric analysis/differential temperature gradient (TGA/DTG) and Fourier transform infrared spectroscopy (FT-IR). The catalysts were evaluated for phenol degradation, and achieved the phenol removal at 80% in 180 minutes.

4.1 Introduction

During the past few years, porous carbon materials have attracted a lot of researchers' interests for their applications such as catalyst supports[1], drug delivery[2] and steal defence system[3]. Porous carbon materials with desired morphology can be used to meet the different requirements[4]. Recently, spherical porous carbon materials are receiving increasing attention in carbon field for their unique physicochemical properties[5].

The treatment and disposal of hazardous organic pollutants in refinery wastewater is one of the most serious environmental problems worldwide[6]. The porous activated carbon is one of the most widely studied and used adsorbents for environmental pollution control[7]. The process of adsorption on activated carbon materials is very efficient to remove dyes from water. A number of industries are using activated carbon to remove phenols occurred in waste water, such as high-temperature[8], coal conversion[9], petroleum resin and plastics[10]. However, drawbacks do exist, in practical application for dispersing media[11].

In this chapter, a unique synthesis of magnetic carbon nanospheres supported Mn catalysts with a two-step hydrothermal method will be presented. The prepared catalysts showed high activity and good magnetic performance in the oxidation of phenol solutions.

4.2. Experimental

4.2.1. Chemicals

Iron (II) chloride tetrahydrate, iron (III) hexahydrate (99.9%), potassium permanganate (99.8%), D-glucose (99.9%) and ammonia solution (28%) were purchased from Sigma – Aldrich. Hydrochloric acid (37%) was received from Fluka. High purity nitrogen gas

(99.999%) was obtained from BOC. All chemicals mentioned above were used as received without any further purification.

4.2.2. Synthesis of magnetic carbon nanospheres (MCS-sep)

The first step was to prepare Fe_3O_4 nanoparticles. Firstly, 0.02 mol iron (III) hexahydrate (99.9%), and 0.01mol iron (II) chloride tetrahydrate were put in 50 mL ultrapure water and stirred for 20 minutes by a magnet rotor until the mixed solids were deeply dissolved. Secondly, nitrogen bubbling was performed (40 mL/min), in 10 minutes, and then 28% ammonia solution was added with a rate of 1 mL/min to make solution pH=10 for synthesis of Fe_3O_4 nanoparticles. After that, nitrogen bubbling was continued for 1 hour (40 mL/min) with stirring and then the resultant was filtered and dried in an oven at 60 ℃ for 12 hours.

The second step was to synthesise the magnetic carbon nanospheres with adding glucose on the previous Fe_3O_4 nanoparticles. The specific procedures are as follows: firstly, 0.25 g Fe_3O_4 particles were put in a beaker, 80mL ultrapure water were added in and followed by 15 minutes' sonicating; secondly, 3.62 g glucose were put to the previous mixture solution with stirring for 10 minutes and then the solution was transferred into a Teflon-lined autoclave (120 ml) and put in an oven at 160 ℃ for 18h. After cooled down to room temperature, the resultant was filtered and washed by ethanol for three times. Finally, the precipitate was put in the oven at 60 ℃ for 12h for drying. The final sample was named as MCS-sep.

4.2.3. Synthesis of MCS supported Mn catalysts (Mn/MCS-sep)

In a typical procedure, firstly, 0.25 g MCS-sep was put in 50 mL ultrapure water, followed by 10 min' sonicating. Secondly, 0.5 g potassium permanganate was added into the above solution and stirred for 10 minutes. Thirdly, 1 ml hydrochloric acid (37%) was added to the above mixture solution and stirred for 20 minutes. After that, the solution was transferred into

a Teflon-lined autoclave (120 mL) and put in an oven at 50 ℃ for 10h. After cooling down to room temperature, the resultant was filtered and washed by ethanol for three times. Finally, the precipitate was put in the oven at 60 ℃ for 12h. The final sample was named as Mn/MCS-sep.

4.2.4. Characterization of materials

Several techniques were used to identify the physicochemical properties of Mn/MCS-sep. The field emission scanning electron microscopy (FE-SEM, Zeiss Neon 40EsB）was used to test its morphological, size and texture information. X-ray diffraction (XRD) was used to study crystallographic structures. The XRD was obtained using a Bruker D8-Advance X-Ray diffractometer with Cu Kα radiation (λ = 1.5418 Å) operated at 40 kV and 30 mA, respectively. The thermogravimetric analysis/differential temperature gradient (TGA/DTG) was used to test the manganese content and thermal stability of Mn/MCS-sep. The TGA/DTG was carried out on a TGA/DSC 1 instrument of Mettler-Toledo under an air flow at a heating rate of 10 ºC/min. The Fourier transform infrared spectroscopy (FT-IR) analysis was performed on a Perkin-Elmer Model FTIR-100 with a MIR detector.

4.2.5. Catalytic oxidation of phenol solutions

The reaction was investigated by oxidation of phenol solutions. The batch experiments were carried out in a 250 mL conical flask which contained 20 ppm phenol solution. The conical flask was put in a water bath at temperature of 25 ℃. Firstly, 0.04 g Mn/MCS–sep catalysts were added to the phenol solution, after stirring for one minute until adsorption-desorption equilibrium on the catalyst was achieved. 0.4 g of oxone was added to the previously mixed solution to activate the reaction. The reaction kept running for 180 minutes. At predetermined time intervals, 1 mL sample was withdrawn with a syringe and filtered into a high performance liquid chromatography (HPLC) vial, after that, 0.5 mL of methanol was added

into the vial to quench the reaction. The water samples were analyzed with a high performance liquid chromatography (HPLC), whose UV detector was set at a wavelength of 270 nm. The mobile phase was made with 30% CH_3CN and 70% deionized water; the flow rate was 1 mL/min. In order to evaluate the catalysts' ability, the catalysts were recycled with magnetic field and washed with ultrapure water for three times.

4.3 Results and discussion

4.3.1 Characterization of the composites

Fig.4.1 shows SEM images, which demonstrate the morphology and composition of the Mn/MCS-sep. The size of the nanoparticle is around 25 nm. Mn particles were expected to homogeneously distribute on the spheres.

Fig.4.2 shows TGA results, which can determine the content of each element in the hybrids. There are three weight loss processes. A slight loss below about 120 ℃ can be assigned to the evaporation of adsorbed water molecules[12]. The TG/DSC curves of the nanocomposites present a characteristic step/peak in the range from 120 to 400 ℃ which can be assigned to the removal of the labile oxygen-containing functional groups on the carbon surface such as –OH and C=O[13]. Then a slight loss occurs from 400 to 590 ℃ which can be assigned to the decomposition of carbon skeleton for the carbon coated on the Fe_3O_4[14]. After the temperature reached 590 ℃, there was no more weight loss.

Fig.4.3 shows FT-IR results, which are used to analyze the functional groups on the Mn/MCS-sep. The bands at 3232, 1744, 1508 and 579cm^{-1} were assigned to –OH, C=O, C-C and Fe-O, respectively[15].

Fig.4.4 shows N_2 adsorption-desorption isotherms and Fig.4.5 shows the pore size distributions of the Mn/MCS-sep. The hysteresis loops in P/P_0 = 0.39-0.99 indicated the

mesoporous structure of the sample. Furthermore, the appearance of H2-type hysteresis loop suggested a porous material with relatively high uniform channel like pores. The specific surface area, pore volume and pore size were 142 m^2/g, 0.12 cm^3/g and 3.4 nm, respectively. Fig.4.6 shows XRD of the crystalline structure of the final samples. The results demonstrate the diffraction peaks at 2θ=30.2°, 35.6°, 43.8°, 57.18° and 63.14°, which present the crystal lanes Fe_3O_4 (220), (311), (400), (422) and (440)[16], respectively. Peaks in Mn/MCS-sep were consistent with the standard XRD data for the inverse spinel structure Fe_3O_4 with lattice constants of a = 8.397 Å (JCPDS No.65-3107)[17]. The Fe_3O_4 nanoparticles' average grain size was 25 nm calculated with the Scherrer's formula[18]. On the other hand, the peaks of Mn were too weak to recognise due to low Mn level.

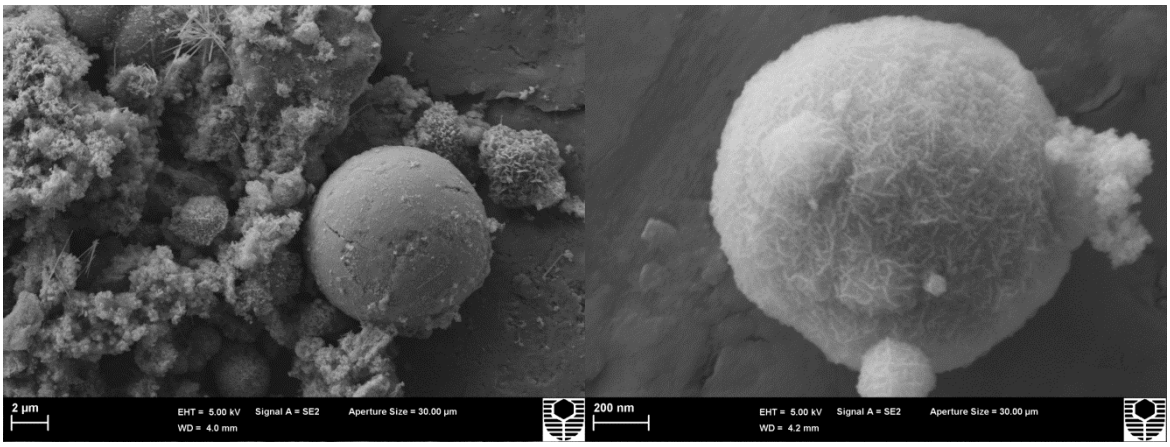

Fig.4.1. SEM images of Mn/MCS-sep.

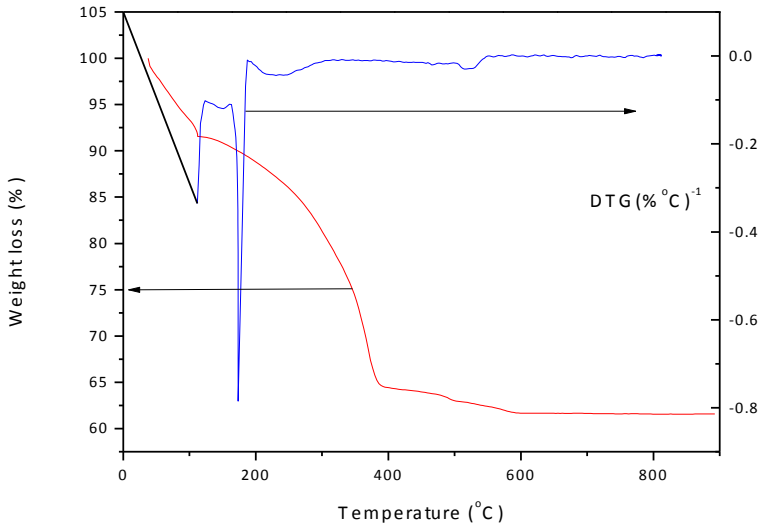

Fig.4.2. TGA and DTG curves of Mn/MCS-sep.

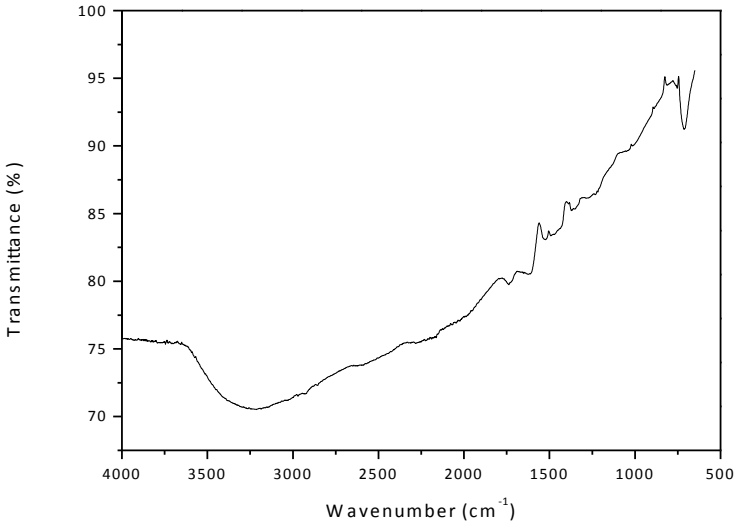

Fig.4.3. FT-IR spectra of Mn/MCS-sep.

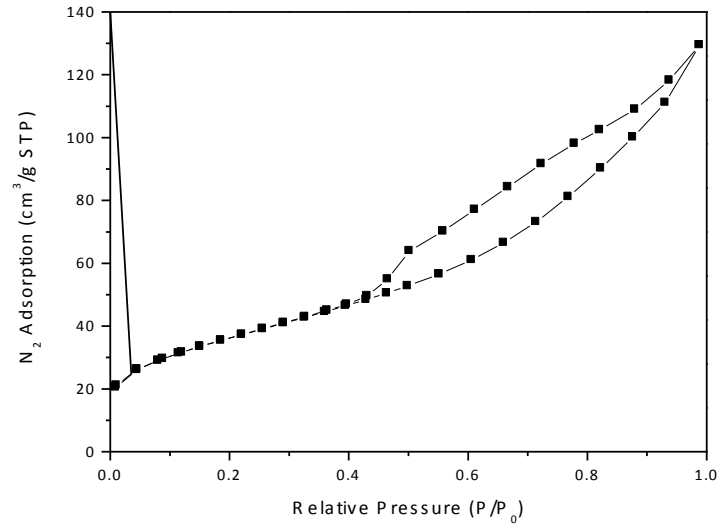

Fig.4.4. N_2 sorption isotherms of Mn/MCS-sep.

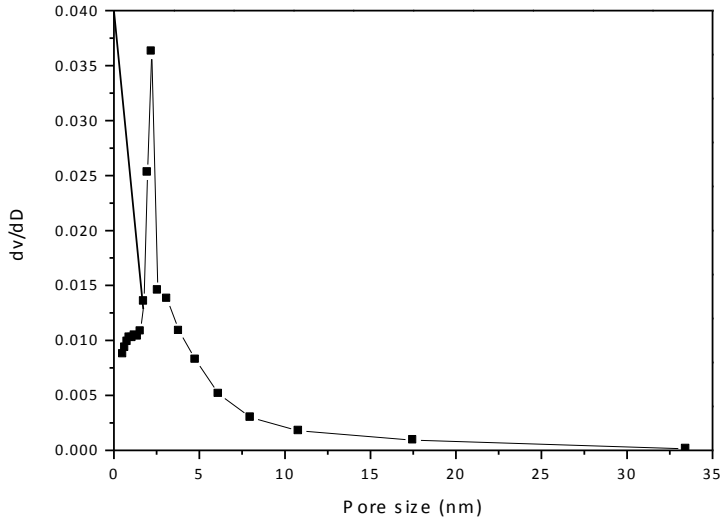

Fig.4.5. Pore size distributions of Mn/MCS-sep.

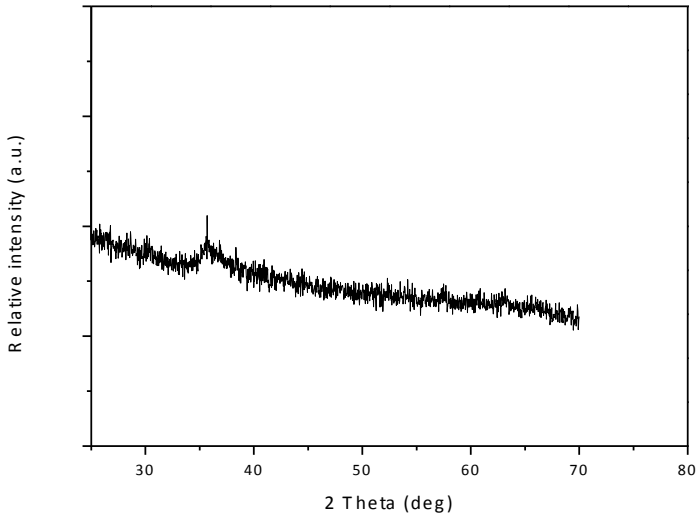

Fig.4.6. XRD patterns of Mn/MCS-sep.

4.3.2 Adsorption and heterogeneous phenol degradation

The catalytic oxidation of phenol is shown in Fig.4.7, which demonstrates the phenol decomposition at different conditions. For the reaction without a catalyst, the final phenol removal rate was about 3% in 180 minutes, which demonstrates PMS itself in homogeneous solution could not induce phenol oxidation. For the adsorption reaction using Mn/MCS-sep only, the final phenol removal rate was less than 1% in 180 minutes, suggesting that phenol adsorption on Mn/MCS-sep is negligible. For the MCS-sep loading with PMS for phenol degradation, the final phenol removal rate was about 10% in 180 minutes and for the Mn/MCS-one, the final phenol removal rate could reach more than 80% in about 180 minutes, suggesting that MCS using as a carrier of manganese oxide will make a more significant contribution to phenol degradation.

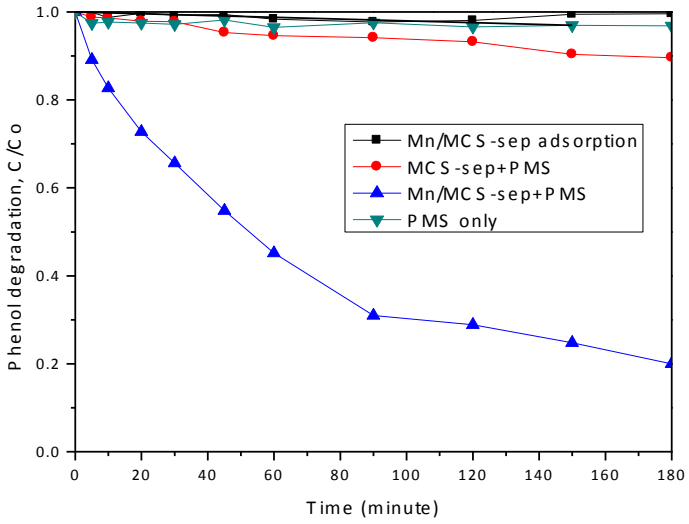

Fig.4.7. Control experiments for phenol removal in different conditions.

4.3.2 Effects of reaction parameters on phenol degradation and stability of the catalysts

Fig.4.8 shows the performance of Mn/MCS-sep catalysts for heterogeneous oxidation of phenol at varying temperatures. It is seen that reaction temperature dramatically affected oxidation efficiency and degradation rate. When reaction took place at 25 ℃, 35 ℃ and 45 ℃, phenol removal rate could reach to 80%, 86% and 99% in 180 minutes, respectively, suggesting that higher temperature can make a more significant contribution to phenol degradation.

It is known that the stability of the catalysts is very important in practical application. Fig.4.9 shows the stability of the Mn/MCS-sep catalysts. In the second time, the phenol degradation rate was 60% in 180 minutes, while in the third run; the phenol degradation rate was less than 40% in 180 minutes, suggesting that the catalytic activities decreased in recycled tests. The decrease in catalytic activity might be attributed to the attachment of reaction intermediates on the catalyst surface which deactivates the correspondent active sites.

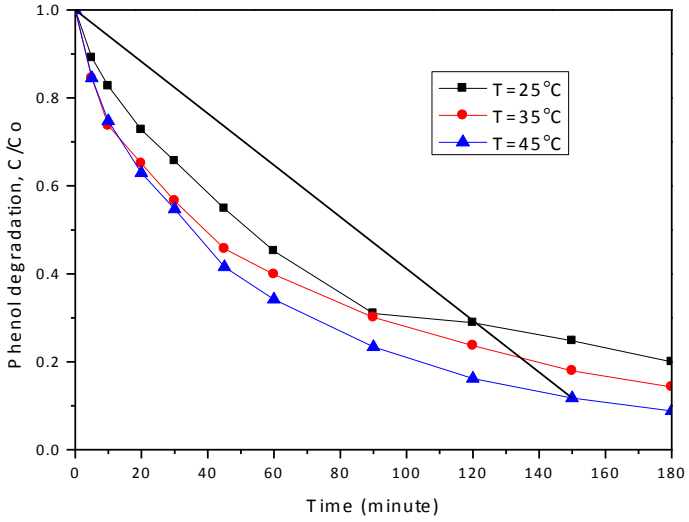

Fig.4.8. Phenol removal at different temperatures.

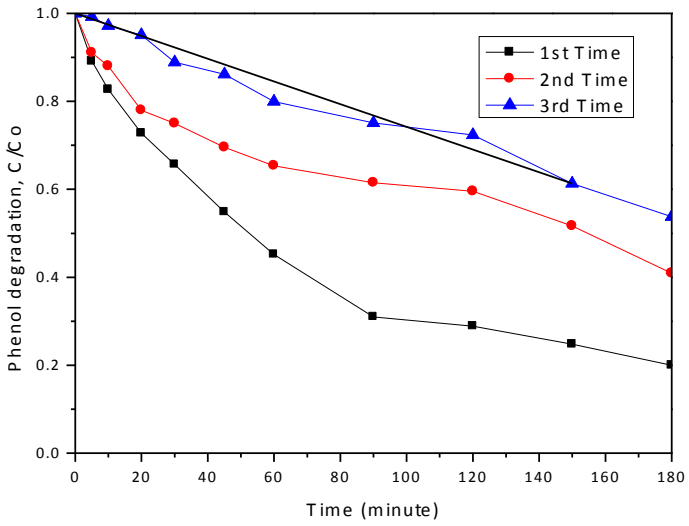

Fig.4.9. Reusability of Mn/MCS-sep catalysts.

4.4 Summary

A two-step hydrothermal method has been successfully adopted to synthesize the magnetic nanocarbon supported Mn nanoparticles, and the catalysts demonstrated to be effective for

activation of PMS in producing oxidative radicals for degradation of phenol. However, compared with the Mn/MCS-one, the Mn/MCS-sep presented worse performance, for the Mn/MCS-one, the final phenol removal rate in 180 minutes at 25 ℃ could reach to 100%, however, for the Mn/MCS-sep, the final phenol removal rate in 180 minutes at 25 ℃ could reach to 80% which presented worse performance. This chapter provided a feasible approach for removal of organic pollutants by magnetically separable catalysts via advanced material design.

4.5 References

1. Yang, C.; Li, D. G., Flexible and foldable supercapacitor electrodes from the porous 3D network of cellulose nanofibers, carbon nanotubes and polyaniline. *Materials Letters* **2015,** *155*, 78-81.

2. Zhou, Y. Q.; Wang, H. G.; Zeng, Y.; Li, C.; Shen, Y.; Chang, J. J.; Duan, Q., Nitrogen-doped porous carbon/Sn composites as high capacity and long life anode materials for lithium-ion batteries. *Materials Letters* **2015,** *155*, 18-22.

3. Wang, H. H.; Peng, H. R.; Li, G. C.; Chen, K. Z., Nitrogen-containing carbon/graphene composite nanosheets with excellent lithium storage performances. *Chemical Engineering Journal* **2015,** *275*, 160-167.

4. (a) Cui, J.; Yang, Y.; Hu, Y.; Li, F., Rice husk based porous carbon loaded with silver nanoparticles by a simple and cost-effective approach and their antibacterial activity. *Journal of colloid and interface science* **2015,** *455*, 117-24; (b) Guan, W.-m.; Li, J.-h.; Qian, T.-t.; Wang, X.; Deng, Y., Preparation of paraffin/expanded vermiculite with enhanced thermal conductivity by implanting network carbon in vermiculite layers. *Chemical Engineering Journal* **2015,** *277*, 56-63; (c) Munoz, M.; de Pedro, Z. M.; Casas, J. A.; Rodriguez, J. J., Preparation of magnetite-based catalysts and their application in heterogeneous Fenton oxidation - A review. *Applied Catalysis B-Environmental* **2015,** *176*, 249-265; (d) Song, Y.; Zuo, L.; Chen, S.; Wu, J.; Hou, H.; Wang, L., Porous Nano-Si/Carbon Derived from Zeolitic Imidazolate Frameworks@Nano-Si as Anode Materials for Lithium-Ion Batteries. *Electrochimica Acta* **2015,** *173*, 588-594; (e) Zhang, M.; Li, R.; Chang, X.; Xue, C.; Gou, X., Hybrid of porous cobalt oxide nanospheres and nitrogen-doped graphene for applications in lithium-ion batteries and oxygen reduction reaction. *Journal of Power Sources* **2015,** *290*, 25-34.

5. (a) Jiang, Z.; Jiang, D.; Yan, Z.; Liu, D.; Qian, K.; Xie, J., A new visible light active multifunctional ternary composite based on TiO2-In2O3 nanocrystals heterojunction decorated porous graphitic carbon nitride for photocatalytic treatment of hazardous pollutant and H-2 evolution. *Applied Catalysis B-Environmental* **2015,** *170*, 195-205; (b) Mao, C.; Kong, A.; Wang, Y.; Bu, X.; Feng, P., MIL-100 derived nitrogen-embodied carbon shells embedded with iron nanoparticles. *Nanoscale* **2015,** *7* (24), 10817-10822; (c) Tan, K. W.; Jung, B.; Werner, J. G.; Rhoades, E. R.; Thompson, M. O.; Wiesner, U., POROUS MATERIALS. Transient laser heating induced hierarchical porous structures from block copolymer-directed self-assembly. *Science (New York, N.Y.)* **2015,** *349* (6243), 54-8; (d) Yan, L.; Xu, Y.; Zhou, M.; Chen, G.; Deng, S.; Smirnov, S.; Luo, H.; Zou, G., Porous TiO2 Conformal Coating on Carbon Nanotubes as Energy Storage Materials. *Electrochimica Acta* **2015,** *169*, 73-81; (e) Yan, X.; Tsotsis, T. T.; Sahimi, M., Fabrication of high-surface area nanoporous SiOC materials using pre-ceramic polymer blends and a sacrificial template. *Microporous and Mesoporous Materials* **2015,** *210*, 77-85.

6. (a) Ahmad, K.; Khan, Z. I.; Ashfaq, A.; Ashraf, M.; Akram, N. A.; Yasmin, S.; Sher, M., Assessment of Heavy Metals and Metalloids in Solanum tuberosum and Pisum sativum Irrigated with Urban Wastewater in the Suburbs of Sargodha City, Pakistan. *Human and Ecological Risk Assessment* **2015,** *21* (4), 1109-1122; (b) Asgari, K.; Cornelis, W. M., Heavy metal accumulation in soils and grains, and health risks associated with use of treated municipal wastewater in subsurface drip irrigation. *Environmental monitoring and assessment* **2015,** *187* (7), 4565-4565; (c) Bunani, S.; Yorukoglu, E.; Yuksel, U.; Kabay, N.; Yuksel, M.; Sert, G., Application of reverse osmosis for reuse of secondary treated urban wastewater in agricultural irrigation. *Desalination* **2015,** *364*, 68-74; (d) Mendoza, A.; Acena, J.; Perez, S.; Lopez de Alda, M.; Barcelo, D.; Gil, A.; Valcarcel, Y., Pharmaceuticals and iodinated contrast media in a hospital wastewater: A case study to analyse their presence and

characterise their environmental risk and hazard. *Environmental research* **2015,** *140*, 225-41; (e) Otero-Gonzalez, L.; Field, J. A.; Calderon, I. A. C.; Aspinwall, C. A.; Shadman, F.; Zeng, C.; Sierra-Alvarez, R., Fate of fluorescent core-shell silica nanoparticles during simulated secondary wastewater treatment. *Water Research* **2015,** *77*, 170-178.

7. (a) Ramasahayam, S. K.; Nasini, U. B.; Shaikh, A. U.; Viswanathan, T., Novel tannin-based Si, P co-doped carbon for supercapacitor applications. *Journal of Power Sources* **2015,** *275*, 835-844; (b) Zyoud, A.; Nassar, H. N. I.; El-Hamouz, A.; Hilal, H. S., Solid olive waste in environmental cleanup: Enhanced nitrite ion removal by ZnCl2-activated carbon. *Journal of Environmental Management* **2015,** *152*, 27-35.

8. Chen, L.; Ji, T.; Brisbin, L.; Zhu, J., Hierarchical Porous and High Surface Area Tubular Carbon as Dye Adsorbent and Capacitor Electrode. *Acs Applied Materials & Interfaces* **2015,** *7* (22), 12230-12237.

9. Joshi, S.; Shrestha, L. K.; Kamachi, Y.; Malgras, V.; Pradhananga, M. A.; Pokhrel, B. P.; Nakato, T.; Pradhananga, R. R.; Ariga, K.; Yamauchi, Y., Synthesis and characterizations of nanoporous carbon derived from Lapsi (Choerospondias axillaris) seed: Effect of carbonization conditions. *Advanced Powder Technology* **2015,** *26* (3), 894-900.

10. Li, M.; Wang, S.; Luo, W.; Xia, H.; Gao, Q.; Zhou, C., Facile synthesis and in situ magnetization of carbon-decorated lignocellulose fiber for highly efficient removal of methylene blue. *Journal of Chemical Technology and Biotechnology* **2015,** *90* (6), 1124-1134.

11. Piotrowska, A.; Kierzek, K.; Machnikowski, J., Effect of PAN Oxidation on the Electrochemical Lithium Insertion/Deinsertion Behavior of Resultant Carbons. *Journal of Chemistry* **2015**.

12. Wang, Y. X.; Sun, H. Q.; Ang, H. M.; Tade, M. O.; Wang, S. B., Synthesis of magnetic core/shell carbon nanosphere supported manganese catalysts for oxidation of

organics in water by peroxymonosulfate. *Journal of Colloid and Interface Science* **2014,** *433*, 68-75.

13. Yan, Z. H.; Cai, Y.; Zhu, G. H.; Yuan, J. B.; Tu, L. D.; Chen, C. Y.; Yao, S. Z., Synthesis of 3-fluorobenzoyl chloride functionalized magnetic sorbent for highly efficient enrichment of perfluorinated compounds from river water samples. *Journal of Chromatography A* **2013,** *1321*, 21-29.

14. Wang, J. H.; Zheng, S. R.; Shao, Y.; Liu, J. L.; Xu, Z. Y.; Zhu, D. Q., Amino-functionalized Fe3O4@SiO2 core-shell magnetic nanomaterial as a novel adsorbent for aqueous heavy metals removal. *Journal of Colloid and Interface Science* **2010,** *349* (1), 293-299.

15. Wang, Y.; Sun, H.; Ang, H. M.; Tade, M. O.; Wang, S., Magnetic Fe3O4/carbon sphere/cobalt composites for catalytic oxidation of phenol solutions with sulfate radicals. *Chemical Engineering Journal* **2014,** *245*, 1-9.

16. Cheng, Y.; Tan, R.; Wang, W.; Guo, Y.; Cui, P.; Song, W., Controllable synthesis and magnetic properties of Fe3O4 and Fe3O4@SiO2 microspheres. *Journal of Materials Science* **2010,** *45* (19), 5347-5352.

17. Dey, R.; Mukherjee, N.; Ahammed, S.; Ranu, B. C., Highly selective reduction of nitroarenes by iron(0) nanoparticles in water. *Chemical Communications* **2012,** *48* (64), 7982-7984.

18. Baby, T. T.; Ramaprabhu, S., SiO2 coated Fe3O4 magnetic nanoparticle dispersed multiwalled carbon nanotubes based amperometric glucose biosensor. *Talanta* **2010,** *80* (5), 2016-2022.

5 Magnetic mesoporous Fe/carbon aerogel structures with enhanced phenol removal efficiency

A B S T R A C T

In this study, magnetic carbon nanospheres supported Mn nanoparticles were synthesized by a one-pot hydrothermal method and self-reduction in N_2 atmosphere with the carbon supplied by hexamethylenetetramine (HMTA). The samples were thoroughly investigated by field emission scanning electron microscopy (FE-SEM), X-Ray diffraction (XRD), thermogravimetric analysis/differential temperature gradient (TGA/DTG) and Fourier transform infrared spectroscopy (FT-IR). The catalysts were evaluated for phenol degradation, which could give effectively phenol decomposition in about 42 minutes.

5.1 Introduction

In recent years, the noble metal nanoparticles have attracted much attention due to their potential[1] and practical applications[2]. Among these materials, Fe_3O_4 nanoparticle is a common magnetic iron oxide[3] that has a cubic inverse spinel structure with oxygen forming a face-centered cubic closed packing[4] and iron cations occupying interstitial sites[5] and octahedral sites[6]. The Fe_3O_4 nanoparticles have drawn much attention for their excellent responses to externally applied magnetic fields while in solution[7]. Therefore, these magnetic nanomaterials can be easily removed from solution with applied external magnetic field[8], avoiding the problems associated with poor separation[9]. However, drawbacks do exist, the Fe_3O_4 nanoparticles are still easily to form aggregates which can decrease their surface area[10]. To solve this problem, the magnetic carbon materials with high surface areas can avoid the aggregation of the nanomaterials. Wu et al. prepared mesoporous magnetic Fe_2O_3@C which shows excellent performance for arsenic capture with remarkable adsorption capacity, easy magnetic separation and good cyclic stability[11]. In addition, Sun et al. successfully synthesized mesoporous Ni/graphitic carbon structures with a specific surface area up to 918 m^2/g[12].

In previous two chapters, we reported that the one-pot hydrothermal method produced better catalysts than the two-step one. In this chapter, we still used the one-pot hydrothermal method; however, we changed the carbon supplier from glucose to hexamethylenetetramine (HMTA). Yi et al. developed the mesoporous Fe/CA structures with carbon supplied from HMTA with high specific surface areas and an excellent response to an applied external magnetic field to provide a feasible approach for wastewater treatment including the removal of arsenic ions[13]. The final catalysts obtained in this process presented higher activity and

better magnetic performance in the reaction of oxidizing phenol solutions than the previous two catalysts.

5.2. Experimental

5.2.1. Chemicals

Ferrous sulfate, hexamethylenetetramines (HMTA) and phenol were purchased from Sigma – Aldrich. High purity nitrogen gas (99.999%) was obtained from BOC. All chemicals mentioned above were used as received without any further purification.

5.2.2. Synthesis of magnetic carbon nanospheres (MCS-HMTA)

In a modified hydrothermal method to synthesize magnetic carbon nanospheres, firstly, 1.1 g ferrous sulfate, 0.187 g hexamethylenetetramine and 0.502 g phenol were put into a conical flask with 60 mL ultrapure water and dissolved completely. Secondly, the mixed solution was transferred to a Teflon-lined autoclave (120 mL) and put in an oven at 140 ℃ for 12h after stirred for 1 minute. Thirdly, the product was washed with ethanol for several times and put in the oven at 60 ℃ for 12h for drying. Lastly, under a nitrogen atmosphere, the as-prepared product was further annealed at 400 ℃ in the tube furnace. The final sample was named as MCS-HMTA.

5.2.3. Synthesis of magnetic nanocatalysts supported Mn catalysts (Mn/MCS-HMTA)

In a typical procedure, firstly, 0.25 g MCS-HMTA was dissolved in 50 mL ultrapure water, followed by 10 min' sonicating. Secondly, 0.5 g potassium permanganate was added into the above solution and stirred for 10 minutes. Thirdly, 1mL hydrochloric acid (37%) was added to the above mixture solution and stirred for 20 minutes. After that, the solution was

transferred into a Teflon-lined autoclave (120 mL) and put in an oven at 50 ℃ for 10h. After cooling down to room temperature, the resultant material was filtered and washed by ethanol for three times. Finally, the precipitate was put in the oven at 60 ℃ for 12h. The final sample was named as Mn/MCS-HMTA.

5.2.4. Characterization of materials

Several techniques were used to identify the physicochemical properties of Mn/MCS-HMTA. The field emission scanning electron microscopy (FE-SEM, Zeiss Neon 40EsB） was used to test its morphological, size and texture information. The X-ray diffraction (XRD) was used to study crystallographic structures. The XRD was obtained using a Bruker D8-Advance X-Ray diffractometer with Cu Kα radiation (λ = 1.5418 Å) operated at 40 kV and 30 mA, respectively. The thermogravimetric analysis/differential temperature gradient (TGA/DTG) was used to test the manganese content and thermal stability of Mn/MCS-HMTA. The TGA/DTG was carried out on a TGA/DSC 1 instrument of Mettler-Toledo under an air flow at a heating rate of 10 ºC/min. The Fourier transform infrared spectroscopy (FT-IR) analysis was performed on a Perkin-Elmer Model FTIR-100 with a MIR detector.

5.2.5. Catalytic oxidation of phenol solutions

The effectiveness of the Mn/MCS-HMTA was investigated by oxidation of phenol solutions. The batch experiments were carried out in a 250 mL conical flask which contained 20 ppm phenol solution. The conical flask was put in a water bath at temperature of 25 ℃. Firstly, 0.04 g Mn/MCS-HMTA catalysts were added to the phenol solution, after stirring for one minute until adsorption-desorption equilibrium on the catalyst was achieved, 0.4 g of oxone was added to the previously mixed solution to activate the reaction. The reaction was kept running for 180 minutes. At predetermined time intervals, 1 mL sample was withdrawn with a syringe and filtered into a high performance liquid chromatography (HPLC) vial, after that,

0.5 mL of methanol was added into the vial to quench the reaction. The water samples were analyzed with a high performance liquid chromatography (HPLC), whose UV detector was set at a wavelength of 270 nm. The mobile phase was made with 30% CH_3CN and 70% deionized water and the flow rate was 1 mL/min. In order to evaluate the catalysts' ability, the annealed catalysts were recycled with magnetic field and washed with ultrapure water for three times.

5.3 Results and discussion

5.3.1 Characterization of the composites

Fig.5.1 shows SEM images, which demonstrate the morphology and composition of the Mn/MCS-HMTA. The size of the nanoparticle is around 1-2 um. Mn particles were expected to be fully covered on the spheres which were better than the previous two samples. And it was observed that 2D sheet-like MnO_x covered the carbon spheres.

Fig.5.2 shows TGA results, which can determine the content of each element in the hybrids. There are five weight loss steps. It presents a slight loss below about 120 ℃ being assigned to the evaporation of adsorbed water molecules[14]. The TGA curve of the nanocomposites present a characteristic step/peak in the range from 120 to 300 ℃ which can be assigned to the removal of the labile oxygen-containing functional groups on the carbon surface such as –OH and C=O[15]. The third weight loss stage is in the range from 300 to 400 ℃ which can be assigned to the decomposition of the carbon skeleton. The fourth weight loss stage is in the range from 400 to 510 ℃ which can be possible assigned to a transformation from MnO_2 to more stable Mn_2O_3. Then a slight loss occurs from 510 to 560 ℃ which can be assigned to a transformation from Fe_3O_4 to more stable Fe_2O_3[16]. After the temperature reached 560 ℃,

there was no more weight loss. According to the TGA results, carbon content included in this as-synthesized Mn/MCS-HMTA sample was calculated to be around 16%.

Fig.5.3 shows the FT-IR results, which are used to analyse the functional groups on the Mn/MCS-HMTA. The bands at 3333, 1613, 1544 and 579cm^{-1} were assigned to –OH, C=O, C-C and Fe-O[17], respectively.

Fig.5.4 shows N_2 adsorption-desorption isotherms and Fig.5.5 shows the pore size distributions of the Mn/MCS-HMTA. The hysteresis loop in P/P_0 = 0.46-0.99 indicated the mesoporous structure of the sample. Furthermore, the appearance of the H2-type hysteresis loop suggested a porous material with relatively high uniform channel like pores. The specific surface area, pore volume and pore size were 56 m^2/g, 0.27 cm^3/g and 12.3 nm, respectively. In terms of pore size distribution, the sample demonstrated a single mode of pore size centering at 7.5 nm.

Fig.5.6 shows the results of XRD of the final samples. The diffraction peaks at 2θ=12.1°, 25° and 37.1°,are referred to the crystal lanes of (001), (002) and (111)[18], respectively. The XRD pattern of Mn/MCS-HMTA was identified to the pure layered birnessite-type MnO_2 (JCPDS No. 80-1098, monoclinic, *C*2/*m*, *a* = 5.15 Å, *b* = 2.84 Å, *c* = 7.17 Å). There are no obvious peaks for Fe_3O_4, it is possible that the peaks of MnO_2 covered the peaks of Fe_3O_4.

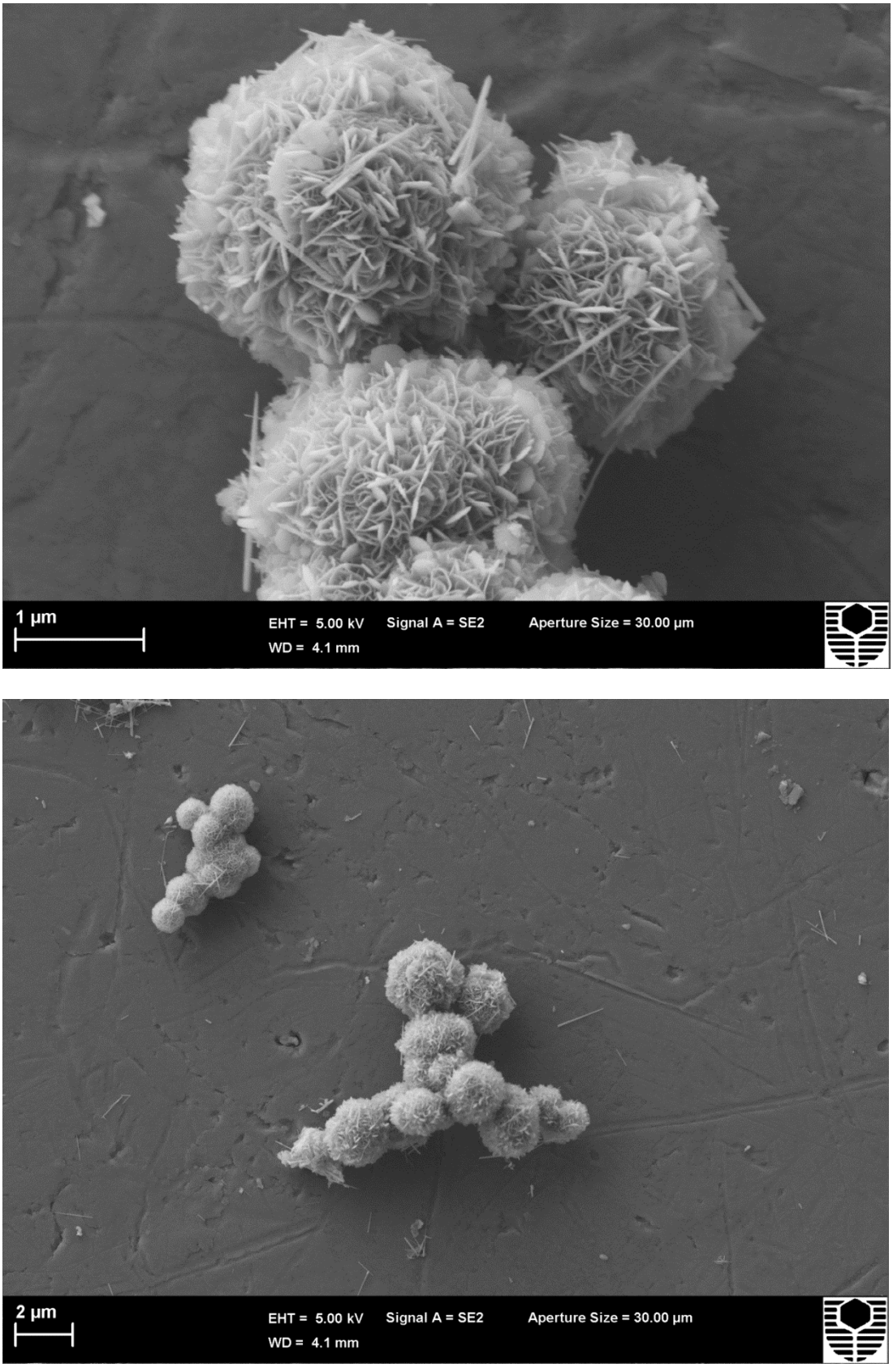

Fig.5.1. SEM images of Mn/MCS-HMTA.

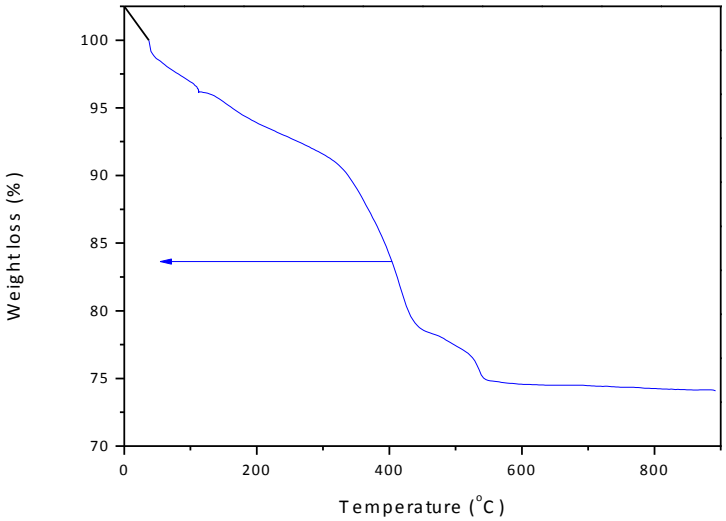

Fig.5.2. TGA curve of Mn/MCS-HMTA.

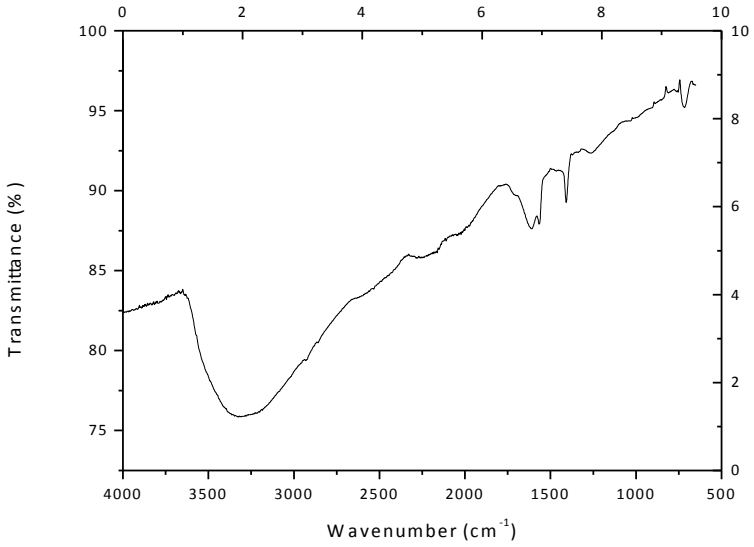

Fig.5.3. FT-IR spectra of Mn/MCS-HMTA.

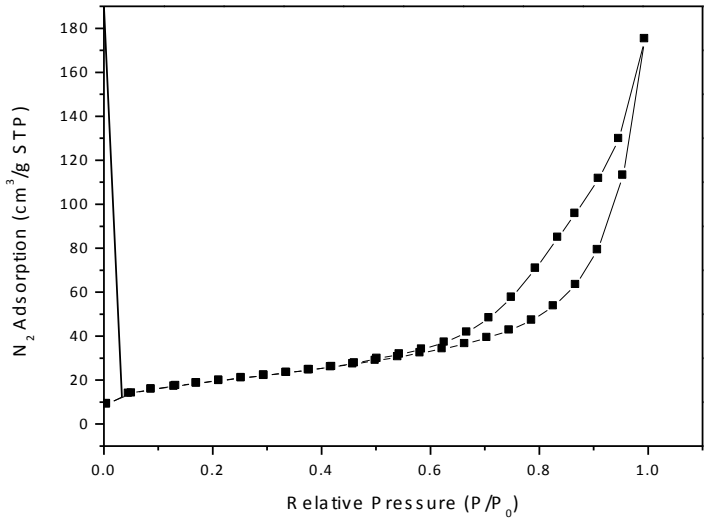

Fig.5.4. N_2 sorption isotherms of Mn/MCS-HMTA.

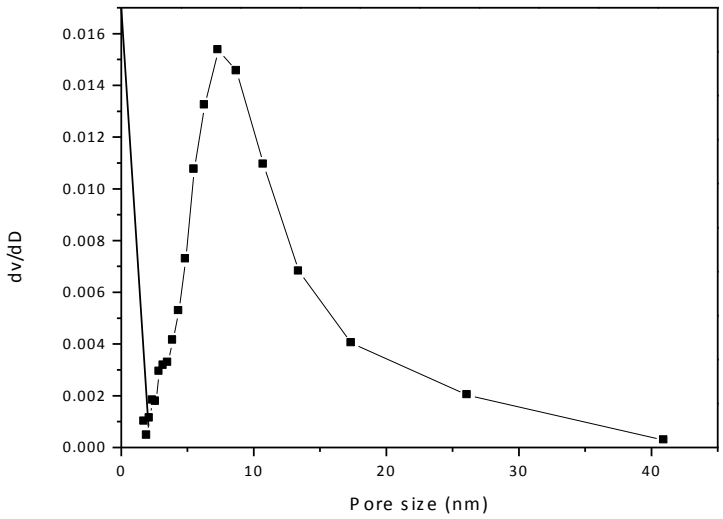

Fig.5.5. Pore size distributions of Mn/MCS-HMTA.

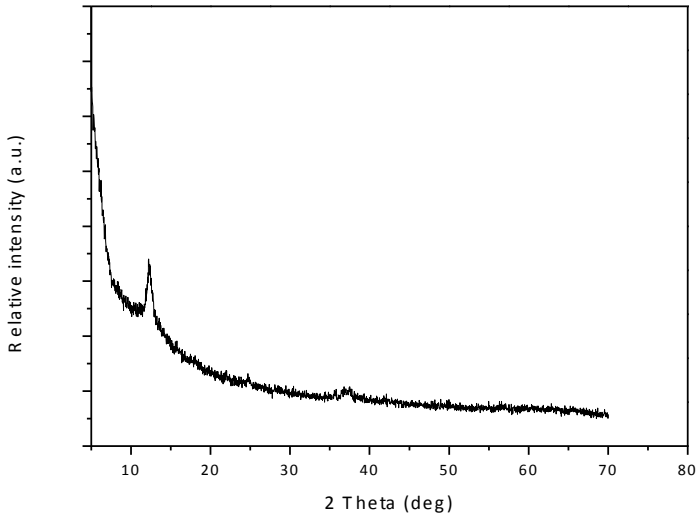

Fig.5.6. XRD patterns of Mn/MCS-HMTA.

5.3.2 Adsorption and heterogeneous phenol degradation

The catalytic oxidation of phenol solutions was carried out and the results are shown in Fig. 5.7, which demonstrates the phenol decomposition at different conditions. For the reaction without a catalyst, the final phenol removal rate was about 3% in 180 minutes, which demonstrates PMS itself in homogeneous solution could not induce phenol oxidation. For the adsorption using Mn/MCS-HMTA only, the final phenol removal rate was less than 4% in 180 minutes, suggesting that phenol adsorption on Mn/MCS-HMTA is negligible. For the MCS-HMTA loading with PMS for phenol degradation, the final phenol removal rate was about 20% in 180 minutes and for the Mn/MCS-HMTA, the final phenol removal rate could reach to 100% in about 42 minutes, suggesting that MCS using as a carrier of manganese oxide will make a more significant contribution to phenol degradation.

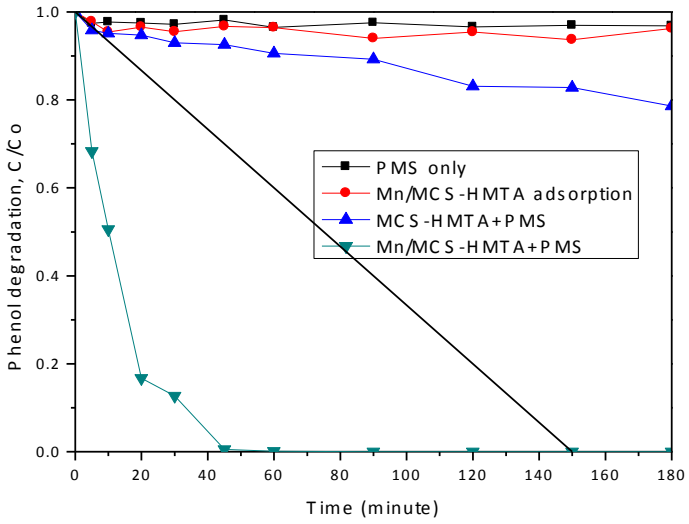

Fig.5.7. Control experiments for phenol removal in different conditions.

5.3.2 Effects of reaction parameters on phenol degradation and stability of the catalysts

In heterogeneous catalytic oxidation of phenol, a lot of conditions can influence the final phenol degradation rate to different extents. This section will show some results of the reaction temperature's effect on phenol degradation.

Fig.5.8 shows the performance of Mn/MCS-HMTA catalysts for heterogeneous oxidation of phenol at varying temperatures. It is seen that reaction temperature dramatically affected oxidation efficiency and degradation rate. When reaction took place at 25 ℃, 35 ℃ and 45 ℃, phenol removal rate could reach to 100% in about 42, 30 and 20 minutes, respectively, suggesting that higher temperature can make a more significant contribution to phenol degradation.

It is known that the stability of the catalysts is very important in practical application. Fig.5.9 shows the stability of the Mn/MCS-HMTA catalysts. In the second time, the phenol degradation rate was about 85% in 180 minutes, while in the third run; the phenol

degradation rate was about 45% in 180 minutes, suggesting that the catalytic activities decreased in recycled tests. The decrease in catalytic activity might be attributed to the attachment of reaction intermediates on the catalyst surface which deactivates the correspondent active sites.

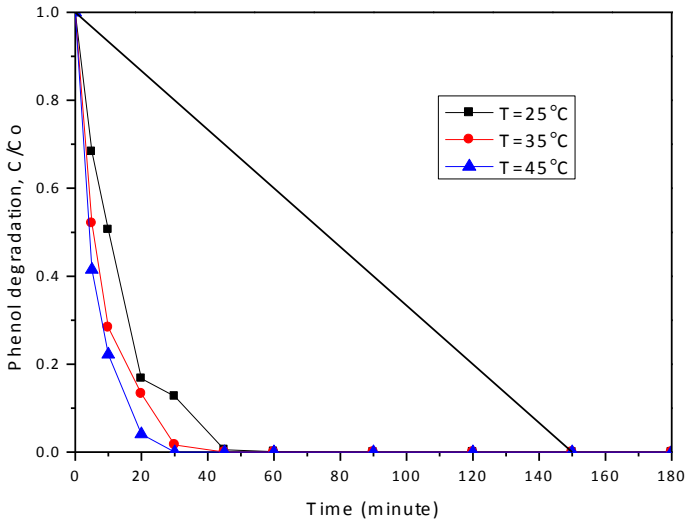

Fig.5.8. Phenol removal at different temperatures

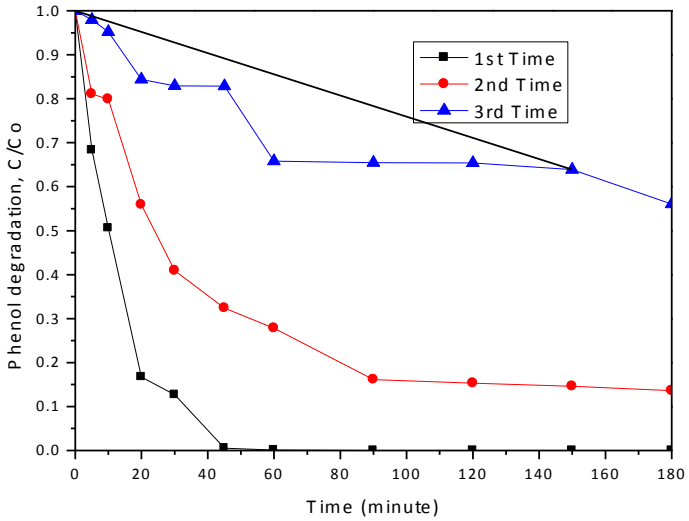

Fig.5.9. Reusability tests of Mn/MCS-HMTA catalysts.

5.4 Summary

Magnetic Mn catalysts were prepared using Fe_3O_4 as the magnetic core with carbon shells supplied by HMTA as a barrier. The Mn/MCS-HMTA is more effective than the Mn/MCS-one and Mn/MCS-sep to activate the PMS in producing oxidative radicals for degradation of phenol, the phenol removal rate of Mn/MCS-HMTA could reach to 100% in 42 minutes, for the Mn/MCS-one, the final phenol removal rate in 180 minutes at 25 ℃ could reach to 100%, however, for the Mn/MCS-sep, the final phenol removal rate in 180 minutes at 25 ℃ could reach to 80%. This chapter provided a feasible approach for removal of organic pollutants by magnetically separable catalysts via advanced material design.

5.5 References

1. (a) Peng, Y.-H.; Tso, C.-p.; Tsai, Y.-c.; Zhuang, C.-m.; Shih, Y.-h., The effect of electrolytes on the aggregation kinetics of three different ZnO nanoparticles in water. *Science of the Total Environment* **2015,** *530*, 183-190; (b) Yuan, G.; Yu, C.; Xia, C.; Gao, L.; Xu, W.; Li, W.; He, J., A simultaneous electrochemical multianalyte immunoassay of high sensitivity C-reactive protein and soluble CD40 ligand based on reduced graphene oxide-tetraethylene pentamine that directly adsorb metal ions as labels. *Biosensors & Bioelectronics* **2015,** *72*, 237-246.

2. (a) El-Atab, N.; Turgut, B. B.; Okyay, A. K.; Nayfeh, M.; Nayfeh, A., Enhanced non-volatile memory characteristics with quattro-layer graphene nanoplatelets vs. 2.85-nm Si nanoparticles with asymmetric Al2O 3/HfO 2 tunnel oxide. *Nanoscale research letters* **2015,** *10* (1), 957-957; (b) Fatima, F.; Bajpai, P.; Pathak, N.; Singh, S.; Priya, S.; Verma, S. R., Antimicrobial and Immunomodulatory efficacy of extracellularly synthesized silver and gold nanoparticles by a novel phosphate solubilizing fungus Bipolaris tetramera. *BMC microbiology* **2015,** *15* (1), 391-391; (c) Kaneti, Y. V.; Yue, J.; Moriceau, J.; Chen, C.; Liu, M.; Yuan, Y.; Jiang, X.; Yu, A., Experimental and theoretical studies on noble metal decorated tin oxide flower-like nanorods with high ethanol sensing performance. *Sensors and Actuators B-Chemical* **2015,** *219*, 83-93; (d) Pouretedal, H. R.; Basati, S., Characterization and Photocatalytic Activity of ZnO, ZnS, ZnO/ZnS, CdO, CdS and CdO/CdS Nanoparticles in Mesoporous SBA-15. *Iranian Journal of Chemistry & Chemical Engineering-International English Edition* **2015,** *34* (1), 11-19.

3. Joshi, M. K.; Pant, H. R.; Liao, N.; Kim, J. H.; Kim, H. J.; Park, C. H.; Kim, C. S., In-situ deposition of silver-iron oxide nanoparticles on the surface of fly ash for water purification. *Journal of Colloid and Interface Science* **2015,** *453*, 159-168.

4. Sun, X.; Ma, Y. Q.; Xu, Y. F.; Xu, S. T.; Geng, B. Q.; Dai, Z. X.; Zheng, G. H., Improved magnetic performance at low and high temperatures in non-exchange-coupling CoFe2O4/CoFe2 nanocomposites. *Journal of Alloys and Compounds* **2015,** *645*, 51-56.

5. Li, K.; Wang, Y.; Huang, M.; Yan, H.; Yang, H.; Xiao, S.; Li, A., Preparation of chitosan-graft-polyacrylamide magnetic composite microspheres for enhanced selective removal of mercury ions from water. *Journal of Colloid and Interface Science* **2015,** *455*, 261-270.

6. Li, T.; Li, Y.; Wu, R.; Zhou, H.; Fang, X.; Su, S.; Xia, A.; Jin, C.; Liu, X., A solution for the preparation of hexagonal M-type SrFe12O19 ferrite using egg-white: Structural and magnetic properties. *Journal of Magnetism and Magnetic Materials* **2015,** *393*, 325-330.

7. (a) Masoudpanah, S. M.; Mirkazemi, S. M.; Shabani, S.; Abadi, P. T. D., The effect of the ethylene glycol to metal nitrate molar ratio on the phase evolution, morphology and magnetic properties of single phase BiFeO3 nanoparticles. *Ceramics International* **2015,** *41* (8), 9642-9646; (b) Mirabi, A.; Rad, A. S.; Khodadad, H., Modified surface based on magnetic nanocomposite of dithiooxamide/Fe3O4 as a sorbent for preconcentration and determination of trace amounts of copper. *Journal of Magnetism and Magnetic Materials* **2015,** *389*, 130-135; (c) Selmi, A.; M'Nassri, R.; Cheikhrouhou-Koubaa, W.; Boudjada, N. C.; Cheikhrouhou, A., Influence of transition metal doping (Fe, Co, Ni and Cr) on magnetic and magnetocaloric properties of Pr0.7Ca0.3MnO3 manganites. *Ceramics International* **2015,** *41* (8), 10177-10184; (d) Yang, H.; Liu, Q.; Masse, S.; Zhang, H.; Li, L.; Coradin, T., Hierarchically-organized, well-dispersed hydroxyapatite-coated magnetic carbon with combined organics and inorganics removal properties. *Chemical Engineering Journal* **2015,** *275*, 152-159.

8. (a) Amir, M.; Sertkol, M.; Baykal, A.; Soezeri, H., Magnetic and Catalytic Properties of CuxFe1-xFe2O4 Nanoparticles. *Journal of Superconductivity and Novel Magnetism* **2015,**

28 (8), 2447-2454; (b) Ivicheva, S. N.; Kargin, Y. F.; Gorelik, V. S., Opal-matrix nanocomposites containing metallic nanoparticles. *Inorganic Materials* **2015,** *51* (8), 840-847; (c) Kakhki, R. M., Application of magnetic nanoparticles modified with cyclodextrins as efficient adsorbents in separation systems. *Journal of Inclusion Phenomena and Macrocyclic Chemistry* **2015,** *82* (3-4), 301-310.

9. (a) Ozcan, F.; Bayrakci, M.; Ertul, S., Synthesis and Preparation of Novel Magnetite Nanoparticles Containing Calix 4 arenes With Different Chelating Group Towards Uranium Anions. *Journal of Macromolecular Science Part a-Pure and Applied Chemistry* **2015,** *52* (8), 599-608; (b) Thangeeswari, T.; Murugasen, P.; Velmurugan, J., Influence of Co and Dy Doping on the Optical and Magnetic Properties of ZnO Nanoparticles for DMS Application. *Journal of Superconductivity and Novel Magnetism* **2015,** *28* (8), 2505-2515; (c) Wang, Y.; Chen, H.; Tang, J.; Ye, G.; Ge, H.; Hu, X., Preparation of magnetic metal organic frameworks adsorbent modified with mercapto groups for the extraction and analysis of lead in food samples by flame atomic absorption spectrometry. *Food Chemistry* **2015,** *181*, 191-197.

10. (a) Beatrice, C.; Di Blasio, G.; Guido, C.; Cannilla, C.; Bonura, G.; Frusteri, F., Mixture of glycerol ethers as diesel bio-derivable oxy-fuel: Impact on combustion and emissions of an automotive engine combustion system. *Applied Energy* **2014,** *132*, 236-247; (b) Claxton, L. D., The history, genotoxicity, and carcinogenicity of carbon-based fuels and their emissions: Part 5. Summary, comparisons, and conclusions. *Mutation Research-Reviews in Mutation Research* **2015,** *763*, 103-147; (c) Oschmann, B.; Tahir, M. N.; Mueller, F.; Bresser, D.; Lieberwirth, I.; Tremel, W.; Passerini, S.; Zentel, R., Precursor Polymers for the Carbon Coating of Au@ZnO Multipods for Application as Active Material in Lithium-Ion Batteries. *Macromolecular Rapid Communications* **2015,** *36* (11), 1075-1082.

11. Wu, Z. X.; Li, W.; Webley, P. A.; Zhao, D. Y., General and Controllable Synthesis of Novel Mesoporous Magnetic Iron Oxide@Carbon Encapsulates for Efficient Arsenic Removal. *Advanced Materials* **2012,** *24* (4), 485-+.

12. Sun, L.; Tian, C.; Wang, L.; Zou, J.; Mu, G.; Fu, H., Magnetically separable porous graphitic carbon with large surface area as excellent adsorbents for metal ions and dye. *Journal of Materials Chemistry* **2011,** *21* (20), 7232-7239.

13. Lin, Y.-F.; Chen, J.-L., Magnetic mesoporous Fe/carbon aerogel structures with enhanced arsenic removal efficiency. *Journal of Colloid and Interface Science* **2014,** *420*, 74-79.

14. Yan, Z. H.; Cai, Y.; Zhu, G. H.; Yuan, J. B.; Tu, L. D.; Chen, C. Y.; Yao, S. Z., Synthesis of 3-fluorobenzoyl chloride functionalized magnetic sorbent for highly efficient enrichment of perfluorinated compounds from river water samples. *Journal of Chromatography A* **2013,** *1321*, 21-29.

15. Duan, X.; Sun, H.; Wang, Y.; Kang, J.; Wang, S., N-Doping-Induced Nonradical Reaction on Single-Walled Carbon Nanotubes for Catalytic Phenol Oxidation. *Acs Catalysis* **2015,** *5* (2), 553-559.

16. Wang, Y.; Sun, H.; Ang, H. M.; Tade, M. O.; Wang, S., Synthesis of magnetic core/shell carbon nanosphere supported manganese catalysts for oxidation of organics in water by peroxymonosulfate. *Journal of Colloid and Interface Science* **2014,** *433*, 68-75.

17. Barazesh, J. M.; Hennebel, T.; Jasper, J. T.; Sedlak, D. L., Modular Advanced Oxidation Process Enabled by Cathodic Hydrogen Peroxide Production. *Environmental Science & Technology* **2015,** *49* (12), 7391-7399.

18. Liang, X.; He, Z.; Wei, G.; Liu, P.; Zhong, Y.; Tan, W.; Du, P.; Zhu, J.; He, H.; Zhang, J., The distinct effects of Mn substitution on the reactivity of magnetite in

heterogeneous Fenton reaction and Pb(II) adsorption. *Journal of Colloid and Interface Science* **2014,** *426*, 181-189.

6. Conclusion and Future work

6.1 Concluding comments

The major objective of this research is to synthesize novel magnetic nanocatalysts to degrade organics via advanced oxidation processes. Several kinds of magnetic nanocatalysts were synthesized with a one-pot or a two-step hydrothermal method, and used for degradation of phenol in aqueous phase. All the catalysts were based on manganese oxide nanoparticles. The magnetic coating of Mn/MCS-one and Mn/MCS-sep was supplied with carbon from glucose, and the coating of Mn/MCS-HMTA was supplied with carbon from hexamethylenetetramine (HMTA). The catalysts of Mn/MCS-one and Mn/MCS-HMTA were synthesized by a one pot hydrothermal method, and the Mn/MCS-sep catalysts were synthesized by a separated hydrothermal method. All of these synthesized catalysts were examined for peroxymonosulfate (PMS, Oxone) activation in the decomposition of phenol. The major outcomes of this research thesis are outlined as below.

6.2 The one-pot hydrothermal method

Magnetic carbon nanocatalysts with high oxidizing performance have been successfully prepared by a one pot hydrothermal method. The Mn/MCS-HMTA can effectively decompose phenol in less than 42 minutes; on the other hand, the Mn/MCS-sep can achieve the phenol removal at only 80% in 180 minutes.

6.3 Effect of Mn on magnetic carbon nanocatalysts

Mn nanoparticles can improve the magnetic carbon nanocatalysts' conductivity and stability to some extent, and oxidizing efficiency of Mn/MCS on phenol decomposition can be much higher than MCS.

6.4 Effect of temperature on phenol degradation of the catalysts

The higher temperature can make a more significant contribution to phenol degradation than the lower temperature. For the Mn/MCS-HMTA, the phenol removal rate could reach 100% in more than 20 minutes shorter at 45 ℃ than the reaction occurred at 25 ℃.

6.5 Recommendation for future work

All the studies focused on the catalytic degradation of phenol in aqueous phase. The results of this study showed that phenol can be successfully oxidized by peroxymonosulfate (PMS) as oxidant. However, detailed study is further required for more comprehensive solutions of removal of organic compounds in wastewater. The recommendations for future research are as follows:

(1) Unexpected toxic intermediates are the main reasons which cause the secondary pollution in wastewater treatment processes. Detailed testing route is highly required to be investigated to determine the intermediates and their adsorption on the catalyst surface.

(2) It is widely accepted that cobalt nanoparticles can improve the magnetic carbon nanocatalysts' stability and efficiency, as a result, in the future research work, the magnetic carbon nanospheres supported Co nanoparticles should be synthesized.

(3) In our study, we only worked on the influence of the temperature on the phenol degradation rate in aqueous solution; however, many studies indicate that the concentrations of PMS and the catalysts concentration can affect the phenol degradation rate as well. Therefore, detailed testing route is highly required to test the effects of other reaction parameters on phenol degradation in the future study.